Late Carboniferous to Permian remagnetization of Devonian limestones in the Ardennes: Role of temperature, fluids, and deformation

T. E. Zegers, M. J. Dekkers, and S. Bailly

Faculty of Earth Sciences, Geodynamic Research Institute, Paleomagnetic Laboratory Fort Hoofddijk, Utrecht University, Utrecht, Netherlands

Received 20 September 2002; revised 20 February 2003; accepted 17 March 2003; published 31 July 2003.

[1] To test various remagnetization mechanisms in unmetamorphosed to very low grade metamorphic carbonates, we integrated paleomagnetic and rock magnetic data of Devonian carbonates with geological observations in the well-studied Rhenohercynian Belt of France and Belgium. Paleomagnetic results from 42 sites show that there are three separate remanence components. Hysteresis measurements that are consistent with unremagnetized limestones and the low paleotemperature of the Boulonnais area (<55°C) indicate that component B is a primary Middle Devonian natural remanent magnetization (NRM). Prefolding to postfolding Carboniferous component C and postfolding Early Permian component P both occur throughout the Ardennes and Brabant Massif. Rock magnetic results indicate that component P is carried by pyrrhotite and component C is carried by a magnetite mix that straddles the single-domain-multidomain grain-size range (10–30 nm). The relative intensity factor, R_i, defined as ln(intensity P/intensity C), shows a marked spatial correlation with the southern of two Mississippi Valley-type (MVT) ore districts. This, in combination with the timing of remagnetization, suggests that component P pyrrhotite formed as a result of percolation of MVT fluids through these carbonates. Fine-grained magnetite formation, as a by-product of smectite-to-illite conversion in the presence of host-rock-buffered internal fluids during deformation, is the most likely remagnetization mechanism for component C. Pressure solution deformation processes may have enhanced the smectite-to-illite conversion and hence remagnetization. *INDEX TERMS:* 1533 Geomagnetism and Paleomagnetism: Remagnetization; 1540 Geomagnetism and Paleomagnetism: Rock and mineral magnetism; 8045 Structural Geology: Role of fluids; 8102 Tectonophysics: Continental contractional orogenic belts; *KEYWORDS:* remagnetization, rock magnetic, deformation, fluids, carbonates, Variscan

Citation: Zegers, T. E., M. J. Dekkers, and S. Bailly, Late Carboniferous to Permian remagnetization of Devonian limestones in the Ardennes: Role of temperature, fluids, and deformation, *J. Geophys. Res.*, *108*(B7), 2357, doi:10.1029/2002JB002213, 2003.

1. Introduction

[2] Remagnetization is ubiquitous in Paleozoic carbonate sedimentary rocks of North America [e.g., *McCabe and Elmore*, 1989; *Elmore et al.*, 1993; *Banerjee et al.*, 1997; *Xu et al.*, 1998] and Europe [*Thominski et al.*, 1993; *McCabe and Channell*, 1994; *Molina Garza and Zijderveld*, 1996; *Weil and van der Voo*, 2002] but is also widespread in Mesozoic carbonates [e.g., *Katz et al.*, 1998; *Jordanova et al.*, 2001]. Although remagnetization in carbonate sequences is now frequently recognized, the mechanism by which it occurs is not well understood. Originally, the remagnetization was thought to be the result of thermoviscous resetting of the natural remanent magnetization (NRM) and was often referred to as the thermoviscous remanent magnetization (TVRM) mechanism [*Horton et al.*, 1984; *Kent*, 1985]. However, it is now widely believed that processes involving the formation of new magnetic minerals, which result in a chemical remanent magnetization (CRM) if they grow sufficiently large, are the cause of most carbonate remagnetization. The current debate revolves around the source, externally or internally derived, and role of fluids as the ultimate cause for the formation of new magnetic minerals. Externally derived basinal orogenic fluids as the cause for the CRM was originally proposed by *Oliver* [1986]. Brines and mineralizing fluids [*Symons and Sangster*, 1992; *Lewchuk and Symons*, 1995] have since been added to the list of possible externally derived remagnetizing fluids. However, the fluid sources may be more complex and fluids may be subsequently altered by fluid-rock interaction. *McCabe and Elmore* [1989] proposed that the migration of hydrocarbons or the maturation of organic matter [*Brothers et al.*, 1996] may play a role in the remagnetization of carbonates. Similarly complex sources

0148-0227/03/2002JB002213$09.00

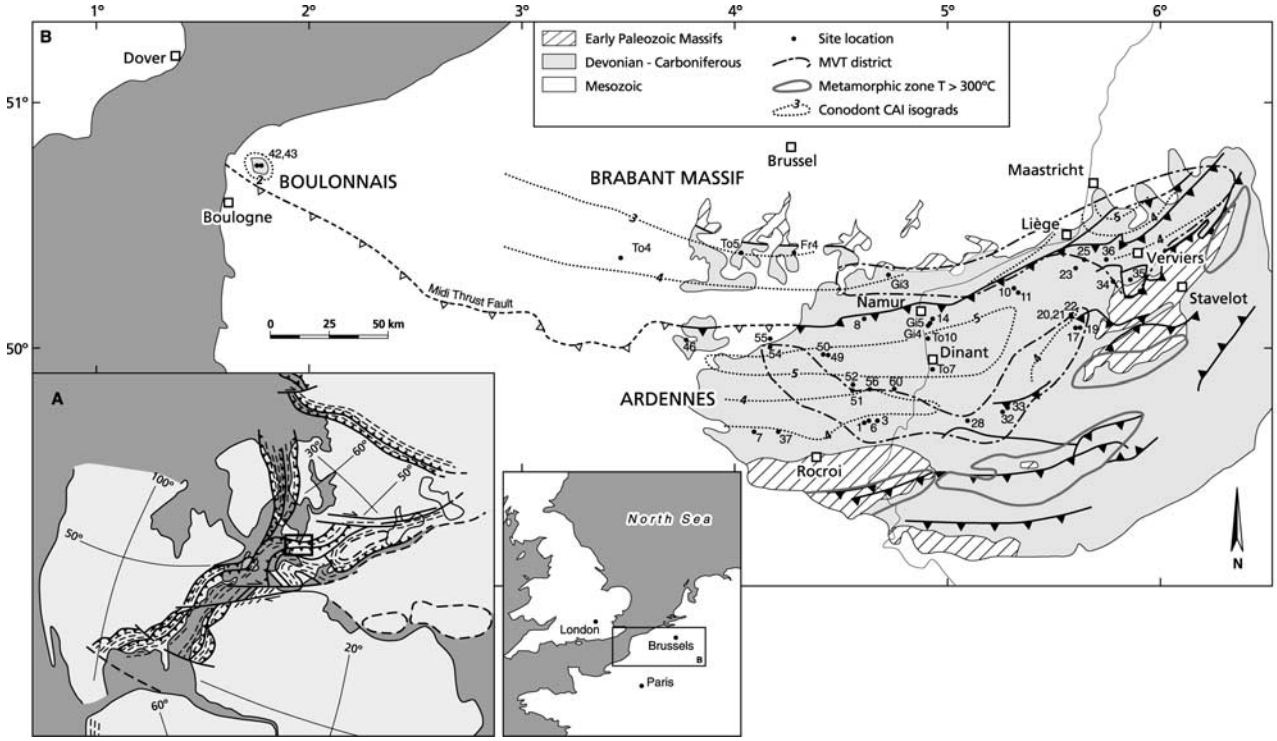

Figure 1. (a) Permian reconstruction of the Variscan orogenic belt in Europe, extending to the Hercynian-Alleghenian belt in the United States [after *Matte*, 1991]. The Rhenohercynian zone is indicated in the rectangle. (b) Map of the study area showing the allochtonous Ardennes fold-and-thrust belt to the south of the main Midi thrust fault and the autochtonous Brabant Massif to the north. The Boulonnais area in northwestern France is part of the Brabant Massif. Metamorphic zones (T > 300°C) are indicated in the area to the south of the early Paleozoic massifs. Conodont color alteration indexes (CAI) values indicate the maximum paleotemperatures for Middle Devonian units [*Helsen*, 1992]. CAI values approximately correspond to paleotemperatures as follows: 2, 55°C; 3, 120°C; 4, 190°C; 5, 300°C. Note the very low CAI value of <2 for the Boulonnais area. Two Mississippi Valley-type ore districts are shown [after *Dejonghe*, 1998], the northern Namur-Verviers district and the southern barite-bearing Dinant district. Site locations and numbers are indicated.

and evolution of fluids may apply to situations where dedolomitization [*Loucks and Elmore*, 1986; *Xu et al.*, 1998], dolomitization [*Hart and Fuller*, 1988], or the conversion of Fe sulfide (pyrite) to magnetite by oxidizing fluids [*Suk et al.*, 1990] are invoked as cause for remagnetization. *Katz et al.* [1998] recently proposed a new remagnetization mechanism, based on the formation of magnetite as a by-product of the conversion of smectite to illite during burial metamorphism. An externally derived fluid is not required in this mechanism and remagnetization can proceed in the presence of local intragranular fluids.

[3] Combinations of several of these mechanisms may operate in a single rock unit at different moments in geological time. This leads to complex NRM behavior that requires an integrated approach for a proper interpretation. The Variscan Belt of Belgium and northern France (Figure 1) can be regarded as the type locality for Paleozoic remagnetized rocks in Europe, and it provides a unique opportunity to study the processes that have led to the remagnetization of Devonian and Carboniferous limestones. Paleomagnetic studies have shown that there are two secondary components in the Devonian and Carboniferous sedimentary rocks: a high temperature (HT [*Molina Garza and Zijderveld*, 1996]) component, or B component [*Thominski et al.*, 1993], with maximum unblocking temperatures between 400 and 580°C, and a low temperature (LT [*Molina Garza and Zijderveld*, 1996]), or A component [*Thominski et al.*, 1993], with unblocking temperatures up to 375°C. The LT component (D = 214°, I = −10°) postdates Variscan folding and is consistent with Early Permian reference poles for Baltica, whereas the HT component (D = 218°, I = 9°) is prefolding to synfolding and consistent with the Carboniferous reference pole for Baltica [*Molina Garza and Zijderveld*, 1996]. In the westernmost Boulonnais area (Figure 1) *Márton et al.* [2000] showed that a third paleomagnetic component (D = 202.7°, I = −10.4° tilt corrected) exists, which they interpreted to be older than the two afore mentioned components but not primary. The cause(s) and mechanism(s) of remagnetization are not yet understood: *Thominski et al.* [1993] did not consider the A component and interpreted the B component to be a TVRM caused by burial during Variscan deformation. *Molina Garza and Zijderveld* [1996] interpreted both the LT and HT components to be CRMs.

[4] The Ardennes and Boulonnais areas have also been the subject of extensive structural, metamorphic, and fluid studies [*Fielitz and Mansy*, 1999; *Muchez et al.*, 2000; *Oncken et al.*, 1999]. This allows the integration of various

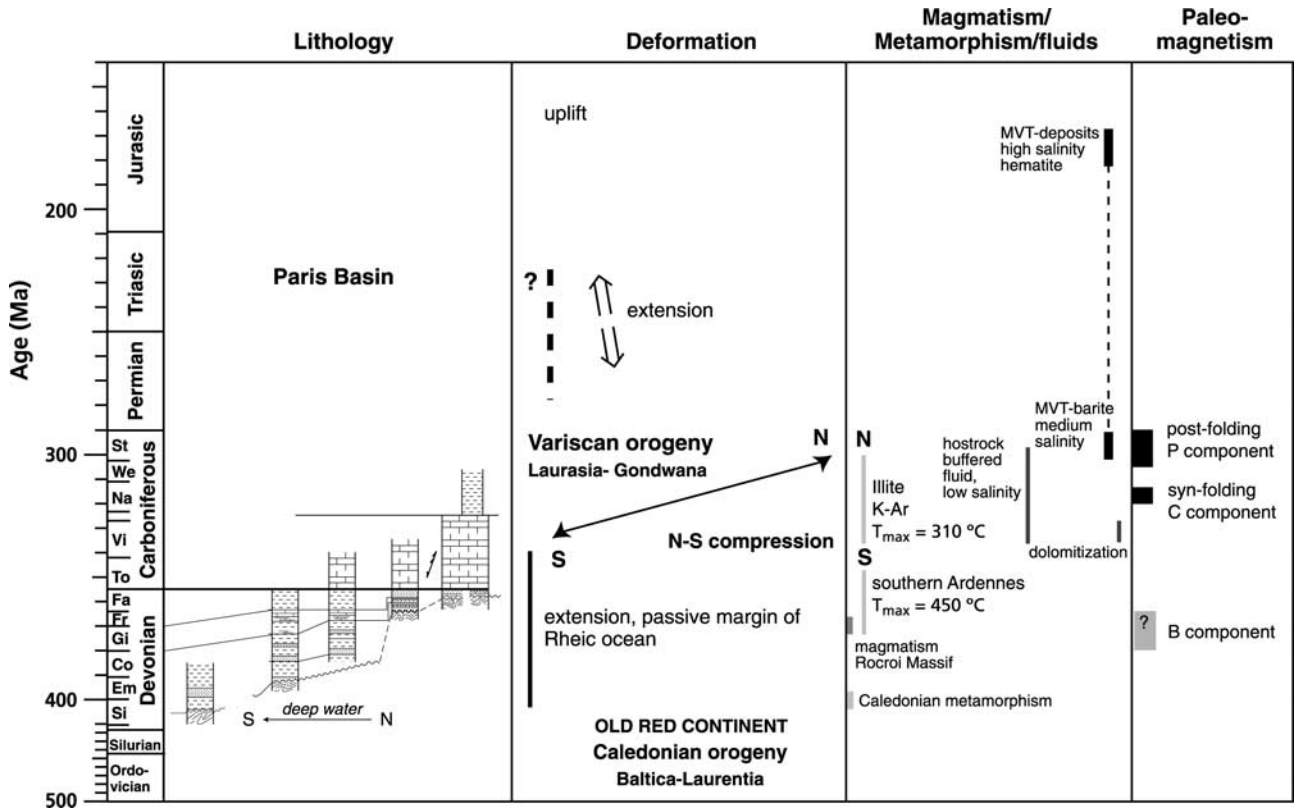

Figure 2. Chronological development of the Rhenohercynian sedimentary basin and subsequent Variscan orogeny in the Ardennes/Brabant Massif area. Devonian ages are from [*Tucker et al.*, 1998] and [*Palmer and Geissman*, 1999]. Si, Siegenian; Em, Emsian; Co, Couvinian; Gi, Givetian; Fr, Frasnian; To, Tournasian; Vi, Visian; Na, Namurian; We, Westphalian; St, Stephanian. Metamorphic events are after *Fielitz and Mansy* [1999], K-Ar illite ages are from *Pique et al.* [1984], fluid composition is from *Heijlen et al.* [2001] and *Muchez et al.* [2000], Mississippi Valley-type deposits are from *Dejonghe* [1998] and *Jochum* [2000], and timing of paleomagnetic components C and P are from *Molina Garza and Zijderveld* [1996].

geological aspects in this part of the Variscan Belt with paleomagnetic and rock magnetic data. As a consequence, various remagnetization hypotheses can be tested for these Paleozoic carbonates. The study by *Molina Garza and Zijderveld* [1996] and a pilot sample set collected by us indicated that Givetian (Middle Devonian) limestones yielded best paleomagnetic results. Numerous natural and quarry outcrops occur in Givetian limestones throughout the study area. Moreover, the study of remagnetization processes in Givetian limestones is favorable because it maximizes the time span between sedimentation and Late Carboniferous and Permian remagnetization in this geologic setting. We started by correlating the timing of different remagnetization events with geological events. In addition, we collected samples from new sites in Givetian limestones and integrated these results with previous paleomagnetic data from Givetian sites [*Molina Garza and Zijderveld*, 1996] to obtain a spatially evenly distributed paleomagnetic and rock magnetic database throughout the Ardennes and Boulonnais. This allowed us to infer spatial and temporal relations between paleomagnetic and rock magnetic attributes with geological features such as deformation, paleotemperature, and the occurrence of Mississippi Valley-type (MVT) ore deposits. The primary goal of this study is to unravel the remagnetization mechanisms that took place in the Givetian limestones.

2. Geological Setting

[5] The Ardennes in northwestern Europe (Figure 1) comprise the western part of the Rhenohercynian zone in the northernmost part of the Variscan orogenic belt. The Variscan orogenic belt is part of a major Paleozoic orogenic belt that extended to the Hercynian-Alleghenian belt in the United States (Figure 1) from ~500 to ~200 Ma. This orogenic belt formed as a result of the convergence and collision between Laurentia-Baltica to the north and Gondwana to the south [*Matte*, 1991].

[6] The geological evolution of the Ardennes is summarized in Figure 2. Passive continental rifting of the Old Red Continent started in the Early Devonian and resulted in the development of a thick Devonian-Carboniferous basin fill, unconformably overlying the variably deformed and metamorphosed lower Paleozoic basement. The outcrops of Paleozoic basement rocks are called ''massifs'' in the Ardennes (Figure 1). A small oceanic basin must have existed to the south of the Ardennes [*Oncken et al.*, 1999] in the Devonian. Subsidence of the Rhenohercynian Basin

occurred diachronously from south to north during the Devonian. Consequently, the Devonian sediment pile is thicker in the south (Figure 2). The closure of the oceanic basin started with southeasterly directed subduction, in the Late Devonian, as indicated by flysh sedimentation and the development of a magmatic arc in the south [*Oncken et al.*, 1999]. The closure of the basin resulted in inversion of the synsedimentary extensional faults and the development of a fold-and-thrust belt in the Rhenohercynian domain. Deformation propagated from south to north from ~325 to ~300 Ma [*Ahrendt et al.*, 1983; *Pique et al.*, 1984] as deduced from K-Ar ages of clay minerals. The northernmost frontal thrust separates the autochtonous Brabant Massif from the allochtonous Ardennes fold-and-thrust belt and is termed the Midi Fault (Figure 1). The main Variscan fold-and-thrust phase was followed by strike-slip deformation along major Variscan thrust zones, starting in the Late Carboniferous [*Oncken et al.*, 1999]. Postorogenic extensional structures have been described in various parts of the Rhenohercynian belt. *Delvaux* [1990] describes postorogenic extensional faults associated with barite veins in the southern Ardennes.

[7] An accurate understanding of the paleotemperature evolution of the Ardennes is important to assess the potential influence of the TVRM remagnetization mechanisms. The Ardennes show a complex pattern of low-grade metamorphic zones, and the timing and geodynamic significance of this pattern has long remained enigmatic. *Fielitz and Mansy* [1999] have summarized all paleotemperature data, including metamorphic studies, illite crystallinity, and conodont colour alteration index (CAI) data. They distinguished three separate metamorphic events, which partly overlap spatially. The first metamorphic event, only recognized in the early Paleozoic massifs (Figures 1 and 2), is pre-Variscan of age (circa 430 Ma). The second metamorphic event affects early Paleozoic and Devonian rocks and shows the highest temperature up to 450°C in the areas south of the early Paleozoic massifs. Isograds of this metamorphic event are folded and offset by Variscan thrust faults, indicating that metamorphism predated Variscan deformation. *Fielitz and Mansy* [1999] interpret this metamorphic event in terms of diastathermal metamorphism (i.e., thermal metamorphism in a static, noncompressive setting) that took place during basin formation in an extensional deformational regime between ~375 and ~310 Ma. The final metamorphic event took place during Variscan deformation, and *Fielitz and Mansy* [1999] consider it to be the thermal expression of crustal thickening by thrusting. Peak thermal conditions during this last event were not higher than 300°C. Areas sampled in this study (Figure 1) mostly fall in the zones of maximum paleotemperatures between 120 and 310°C, based on CAI values (3 to 5) and illite crystallinity data [*Fielitz and Mansy*, 1999]. The exception is the Boulonnais area, the westernmost area that was sampled (Figure 1). Here CAIs range between 1.5 and 2, indicating a maximum temperature of 50 to 55°C only [*Helsen*, 1992].

[8] For a proper assessment of the importance of the various CRM remagnetization mechanisms, information concerning fluids is essential. Fluids are held responsible for the deposition of MVT deposits, but they also play an important role in the advective distribution of heat. Hence they are related to the metamorphic development of foreland fold-and-thrust belts. Extensive fluid studies in the Ardennes area [*Nielsen et al.*, 1998; *Kenis et al.*, 2000; *Muchez et al.*, 2000; *Schroyen*, 2000] have shown that at least three different types of fluids can be distinguished on the basis of their salinity. Low salinity (2–7.8 eq wt % NaCl, homogenization temperature 120–140°C) fluid inclusions in carbonate veins formed during Variscan deformation indicate thermal and chemical equilibrium between fluid and the host rock, probably in a closed system. A second younger group of fluid inclusions in calcite veins has a salinity of 12–16 eq wt % NaCl and homogenization temperatures of 140 to 160°C. These fluids are thought to have originated from the metamorphic zone to the south of the Ardennes, migrating toward the north during the late stages of Variscan deformation. A third group of post-Variscan fluids is characterized by high salinity (18.6–22.9 eq wt % NaCl) and relatively high homogenization temperatures of about 180°C. It is this last group that is associated with the major Zn-Pb MVT deposits [*Heijlen et al.*, 2001] that occur in the northern MVT district, the Namur-Verviers District [*Dejonghe*, 1998] (Figure 1). This district contains the largest Pb-Zn deposits, consisting of mainly sphalerite, galena and pyrite. A second MVT district occurs parallel, but further to the south. This southern Dinant District includes minor Pb-Zn deposits that typically contain barite and fluorite. It is not clear what the composition is of the fluids associated with the Dinant District.

3. Sampling and Methods

[9] Samples from 42 sites from Devonian limestones throughout the Ardennes and the Boulonnais areas (mostly drilled cores, but also oriented hand samples) were collected and analyzed (Figure 1). To study the geographic variation in magnetic parameters we aimed at selecting Givetian sites with an even geographic distribution. This resulted in 32 new sampling sites in the Ardennes and 2 in the Boulonnais area. In addition we used data from 8 sites in Givetian to Lower Carboniferous limestones sampled by *Molina Garza and Zijderveld* [1996] (Table 1).

[10] The standard-sized specimens were thermally demagnetized in noninductive furnaces in 15 to 20 temperature steps up to 700°C. The NRM was measured with a 2G Enterprises DC-SQUID cryogenic magnetometer (noise level 3×10^{-7} A m^{-1} for a 10 cm^3 specimen). Initial NRM intensities ranged from 3 to 100 mA m^{-1}, i.e., typically 10^{+4} to 10^{+5} times above the noise level of the magnetometer. Vectorial components were identified by inspection of orthogonal demagnetization diagrams [*Zijderveld*, 1967], and directions were calculated using principal component analysis [*Kirschvink*, 1980].

[11] In the case of multicomponent demagnetization trajectories, the demagnetization behavior was analyzed with a method described by *Van Velzen and Zijderveld* [1995] and formalized in the program PALDKPRO. This allows the evaluation of the intensity decay behavior of individual NRM components. In particular the initial intensity of each individual component can be derived, which enables the calculation of the R_i factor, defined here as the natural logarithm of the ratio of the low

Table 1. Site Mean Directions and Ri Factor for All Sites[a]

					P Component (in Situ)				C Component (in Situ)				Bedding		C Tectonic				
Site	Latitude, N	Longitude, E	Age	n/N	D	I	α_{95}	k	D	I	α_{95}	k	Strike	Dip	D	I	N_r	ln(Ip/Ic)	σ
Ardennes and Brabant Massif																			
TB1	50°04′38″	4°35′07″	Givetian	7/7	220	−10.4	3.7	264	201	0.6	9.3	43.2	257	83			5	1.99	0.50
TB3	50°05′27″	4°38′25″	Couvinian	4/4	215	−17.5	14.5	40.9					253	88				10.00	
TB6	50°05′19″	4°35′59″	Givetian	4/5	200	−6.3	20.1	21.8	190	20.6	6.1	408	250	59			3	0.30	0.20
TB7	50°03′16″	4°04′44″	Givetian	4/4	203	−0.9	14	44.3	213	−20	12.1	58.5	249	63	212.9	19.3	3	−1.04	0.92
TB8	50°23′19″	4°34′46″	Givetian	3/3	209	−1.7	12.7	95.9	232	−29	11.4	118	232	91	203.1	0.4	3	−0.08	0.19
TB10	50°29′50″	5°15′37″	Givetian	3/4	193	−4.2	5.2	558	211	31.8	23.1	29.4	68	35	200.9	7.8	3	−1.13	0.42
TB11	50°29′06″	5°15′57″	Givetian	5/5	195	−2.1	9.4	66.8	196	−21	8.3	86.6	263	39	195.3	14.8	5	−0.22	0.20
TB14	50°24′58″	4°54′35″	Breccia	2/4	200	−1.9			234	−32							3	−0.03	0.32
TB17	50°21′29″	5°33′05″	Givetian	3/4	187	−2.2	16.6	56.2	193	10.6	6.1	412	133	37			3	−0.20	0.30
TB19	50°21′26″	5°34′28″	Givetian	5/7	195	1.2	8.5	81.5	185	8.5	4.4	301	variable				5	1.10	0.53
TB20	50°23′33″	5°32′12″	Givetian	9/9	194	−1	6.9	57	196	12.5	9.5	30.2	variable				8	−0.23	0.32
TB21	50°23′29″	5°32′23″	Famenian	3/8	191[b]		9.6	15.5	64.4	197	55.3	26.9	22.1	244	89	308.6	25.6	3	−0.02	0.16
TB22	50°23′48″	5°31′59″	Givetian	2/3	190	−2.2			195	19.3			43	37			2	0.67	0.44
TB23	50°32′01″	5°32′41″	Givetian	4/4	210[b]		10.4	9	106	218	31.4	8.9	106	67	61	205.9	−6.0	3	−0.54	0.24
TB25	50°33′32″	5°35′02″	Givetian	3/3	208	1.4	12.2	104	193	−23	8.5	211	265	42	192.4	17.4	3	0.09	0.12
TB28A/B	50°05′17″	5°03′16″	Givetian	5/5	204	−19.4	6.5	138	203	2.1	17	21.2	264	84			6	1.04	0.58
TB32	50°06′42″	5°12′32″	Givetian	4/5	199[b]		12.1	7.9	137	215	32.1	26.6	12.9	94	54			2	0.76	0.29
TB33	50°07′39″	5°14′19″	Givetian	5/5	199	−9	7.8	97.3	199	10	9	73.7	234	65			5	1.13	0.45
TB34	50°29′06″	5°43′07″	Givetian	4/5	204	−6.7	5.2	314	197	14.7	7.2	166	193	30	204.2	10.5	5	−0.04	0.17
Tb35	50°29′52″	5°47′53″	Frasnian	6/6	193	−7.6	7.3	85.7	244	−25	14.2	76.5	56	58	261.1[b]	−6.7	4	0.01	0.09
TB36	50°33′45″	5°41′37″	Givetian	5/5	204	−6.9	8.7	78.7	225	−46	5.8	174	254	85	203.1	15.9	5	−0.09	0.14
TB37	50°03′33″	4°10′29″	Givetian	6/6	211	−6.8	11.5	65.3	231	2.2	6.3	114	267	36			4	0.64	0.51
TB46A	50°13′20″	3°43′00″	Givetian	9/11	205	−1.1	6.6	61	[b]				variable		222.2	14	4	0.59	0.17
TB48	50°16′19″	4°24′21″	Givetian	6/6	204	0.1	14.9	39	248	42.4	9.7	48.6	91	64	223.7	1.8	6	0.88	0.24
TB49	50°16′29″	4°25′37″	Givetian	8/8	203	−2.7	8	133	235	36.4	5.9	89.4	90	64	222.0	−8.7	5	0.36	0.21
TB50	50°16′28″	4°24′22″	Givetian	4/4	214	−10.2	8.9	108	235	−35	8.1	131	267	52	221.2	−0.4	4	0.55	0.33
TB51	50°10′51″	4°31′47″	Givetian	5/7	204	−14.6	8.2	89	238	15.4	12.9	36.2	101	22	236.0	0.0	3	0.82	0.40
TB52	50°10′59″	4°31′49″	Givetian	7/7	203	−12.1	6	102	232	−19	5.3	130	267	53	229.9	13.4	5	0.04	0.21
TB54	50°18′02″	4°09′28″	Givetian	7/7	211	−1.3	8.7	49.4	233	−20	8	58	286	58	234.7	27.0	2	0.26	0.14
TB55	50°19′03″	4°08′57″	Frasnian	7/7	209	−0.4	3.6	286	240	43.6	6.6	104	90	79	220.1	−12.8	5	0.58	0.32
TB56	50°10′48″	4°36′16″	Givetian	7/7	209	−3.2	7.9	58.8	234	39.7	7.4	67.3	77	61	212.1	2.6	6	0.06	0.30
TB60	50°10′13″	4°43′24″	Frasnian	4/4	206	−1.9	13.6	46.9	251	56.1	11.6	63.7	102	74	220.5	−2.9	3	−0.01	0.17
Molina Garza and Zijderveld [1996]																			
Gi3	50°31′43″	4°30′07″	Givetian	8/14	196	−9	6.3	79.2	205	14.7	7.8	88.5	98	9	204.7	6.4	2	−0.02	0.29
Gi4	50°22′43″	4°53′53″	Givetian	8/18	216	−10.7	3.3	206	227	−39	3.1	315	288	65	221.4	20.2	4	−0.64	0.35
Gi5	50°24′08″	4°53′54″	Givetian	6/11	213	−6.3	5.1	140	226	39.7	7.8	96.9	80	46	212.4	9.1	2	−0.02	0.02
To7	50°13′55″	4°53′44″	Tournasian	4/8	211	−11.5	5.1	331	235	35.8	15.7	62.9	107	33	227.5	8.3	2	−0.04	0.05
To10	50°19′08″	4°52′43″	Tournasian	4/8	220	−7.3	15.6	35.9	252	67.3	3.3	1453	104	76	213.2	1.5	4	−0.26	0.08
Fr4	50°34′53″	4°15′15″	Frasnian	12/27	197	−13.4	3.9	67.4	205	6.5	3.9	145	102	8	204.6	8.3	2	−0.80	0.43
To5	50°34′37″	4°00′41″	Tournasian	5/6	208	−10	5.1	229	217	12.4	5.3	210	106	12	216.5	1.6	2	−1.41	0.01
To4	50°35′35″	3°51′41″	Tournasian	7/8					209	4.1	1.9	988	hor		[b]			−10.00	
Boulonnais																			
TB42	50°50′30″	1°47′30″	Givetian	6/11	197	17.1	10.8	39.4					135	25	198.6	−5.2			
TB43	50°50′30″	1°47′30″	Givetian	8/9	208	16.9	6.6	71.6					143	26	208.2	−8.1			

[a]N, number of samples measured; n, number of samples used in calculation of site mean directions; N_r, number of samples used to determine the site-mean R_i factor; D, declination; I, inclination; α_{95}, semiangle of the cone of 95% confidence; k, precision parameter; R_i, site-mean relative intensity factor ln (intensity P/intensity C); σ, standard deviation of R_i.

[b]Outliers not included in Figure 4a.

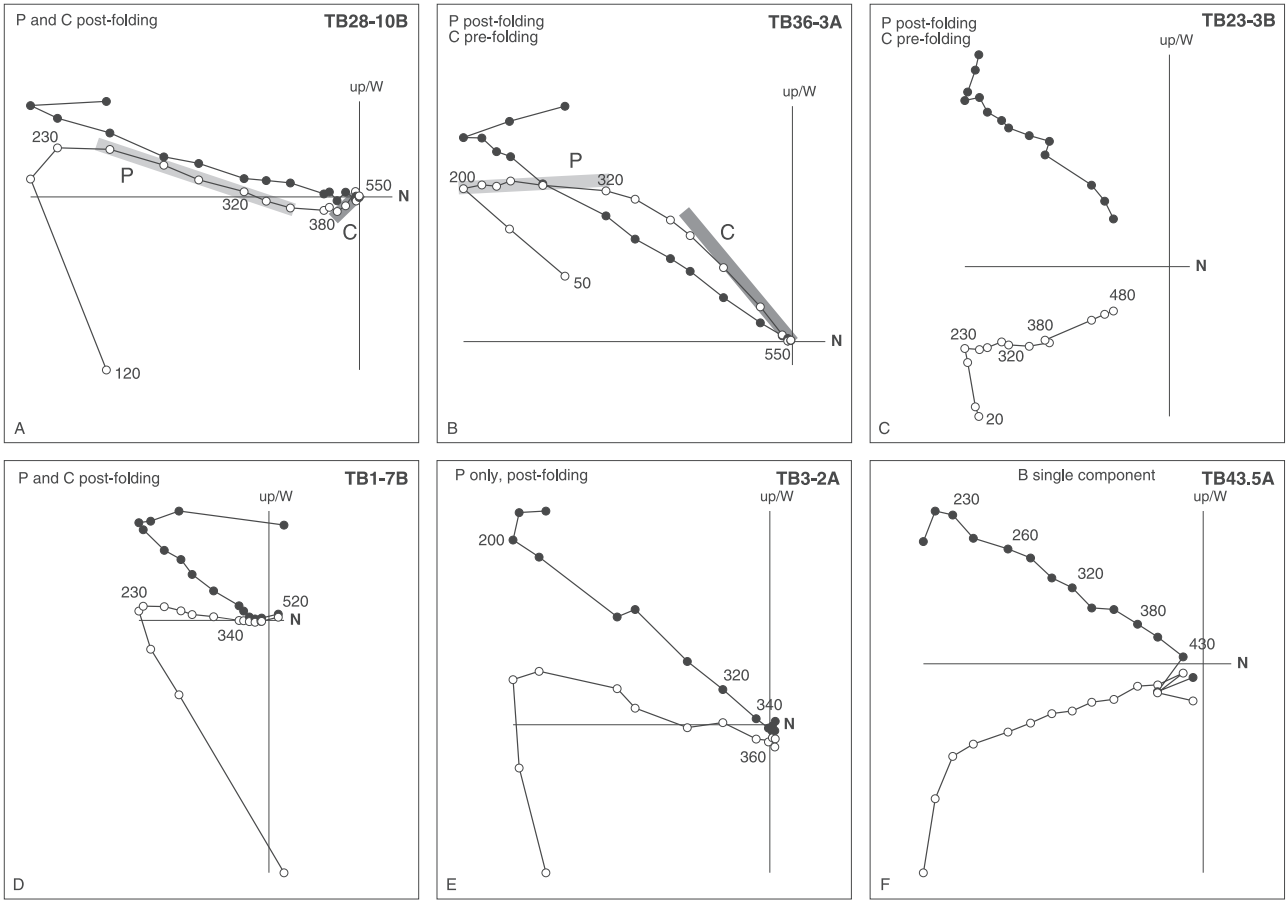

Figure 3. Orthogonal thermal demagnetization diagrams (all in situ coordinates). Open (solid) circles represent projections onto the vertical (horizontal) plane. Demagnetization temperatures are given in degrees Celsius. All diagrams show a modern VRM up to temperatures of 230°C. (a) to (d) Two remagnetized NRM components in Givetian limestones: P with unblocking temperatures up to 360°C and C with unblocking temperatures up to 520°C. In Figures 3a and 3d both components P and C are postfolding. In Figures 3b and 3c, component P is postfolding and component C is prefolding. (e) Only component P. The specimen was collected in a Couvinian limestone next to a barite vein. (f) Single, potentially primary, NRM component B of a Givetian specimen from the Boulonnais area.

temperature (P) over the high temperature (C) component. Under the proviso that one vector (component) is well determined, the direction of the other vector and intensity decay of both vectors can be calculated from input demagnetization data by fitting the best plane through the NRM vectors determined by each temperature step. In the Ardennes samples the high temperature component is usually best defined and is used as the fixed component. Using least squares minimization, the program calculates the best fitting plane, the direction of the low temperature component, and the intensity decay of both components. As a starting point for the iteration an approximate direction of the low temperature component is entered. The results of the fitting depends on the choice of the fixed component. This method was only used for specimens where both components are sufficiently well determined by a linear segment of at least four datapoints.

[12] To provide information on NRM carriers, induced anhysteric remanent magnetization (ARM) and three-dimensional isothermal remanent magnetization (3-D IRM) components [*Lowrie*, 1990] were stepwise thermally demagnetized. Thermomagnetic runs on selected samples were performed and hysteresis loops were determined at room temperature. ARM was acquired in a laboratory-built alternating field demagnetization coil with peak alternating fields of 300 mT; the DC bias field was 32 μT. Three-dimensional IRM was introduced in the samples with a PM4 pulse magnetizer designed by Harald Boehnel; IRM acquisition fields were 2 T, 350 mT, and 80 mT. Remanences were measured with the DC-SQUID magnetometer. Thermomagnetic runs were performed on bulk samples with a modified horizontal translation Curie balance, which uses a sinusoidally cycling applied magnetic field instead of a steady field [*Mullender et al.*, 1993].

[13] Hysteresis loops were measured with an alternating gradient magnetometer (Micromag, Model M2900). The sensitivity of the instrument is 1 nAm^2, typical data values were at least one order of magnitude higher. The accuracy of each measurement is ±2% versus the calibration. The maximum applied field used was 1 T and the field increment was 1 mT. Measurements were corrected for paramagnetic or diamagnetic slope. Backfield demagnetization was

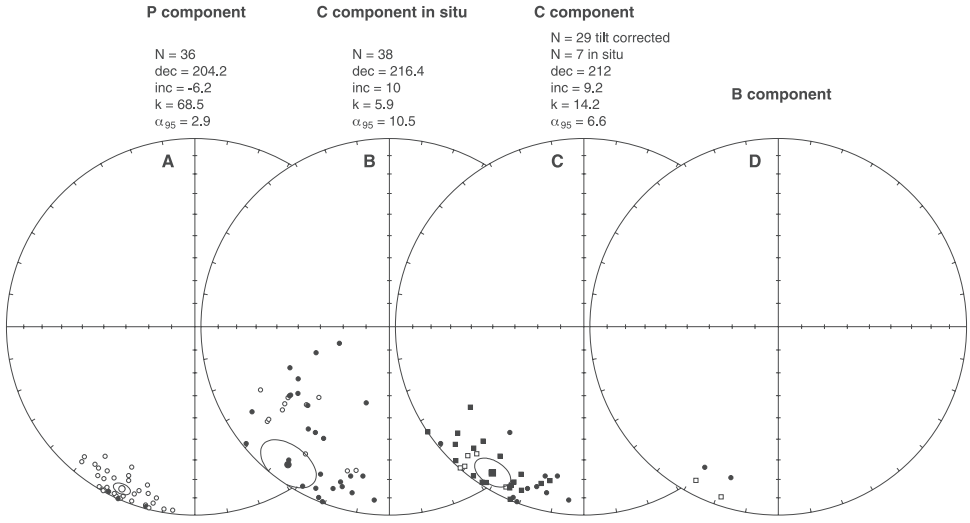

Figure 4. Equal-area stereonet projections of site-mean directions (see also Table 1). Open (solid) symbols represent upper (lower) hemisphere projections. (a)–(c) Site-mean directions for sites in the Ardennes and Brabant Massif. Figure 4a is component P in situ. Figure 4b is component C in situ. Figure 4c is component C in situ (circles) for sites in the southern Ardennes, where component C is postfolding, and in tectonic coordinates (squares) for sites where component C is prefolding. (d) Site-mean directions of component B from two sites in Givetian limestones in the Boulonnais area. Both in situ (circles) and tilt-corrected (squares) coordinates are shown.

performed with the same magnetometer with a field increments of 1 mT to a maximum field of 1 T to determine the coercivity of remanence.

4. Results

4.1. NRM Components

[14] Samples in this study come from sites from three domains within the study area. We define the Ardennes domain as the region to the south of the Midi Fault, the Brabant Massif domain as the region north of the Midi Fault, and the Boulonnais domain as the westernmost outcrop of Paleozoic rocks in Belgium and France (Figure 1).

[15] Thermal demagnetization up to 230°C removes a NRM component with a northerly declination and positive inclination in most specimens from all locations (Figure 3). This magnetization is interpreted to be a modern viscous remanent magnetization (VRM). After removal of the VRM, most specimens from the Ardennes and Brabant Massif domains are characterized by two other NRM components (Table 1). The component with the lowest maximum unblocking temperature, removed between ~230 and ~400°C (Figures 3a–3e), always has southeasterly declinations and shallow negative inclinations (Figure 4a). Its direction is consistent with the low temperature Late Carboniferous to Permian remagnetization described by *Molina*

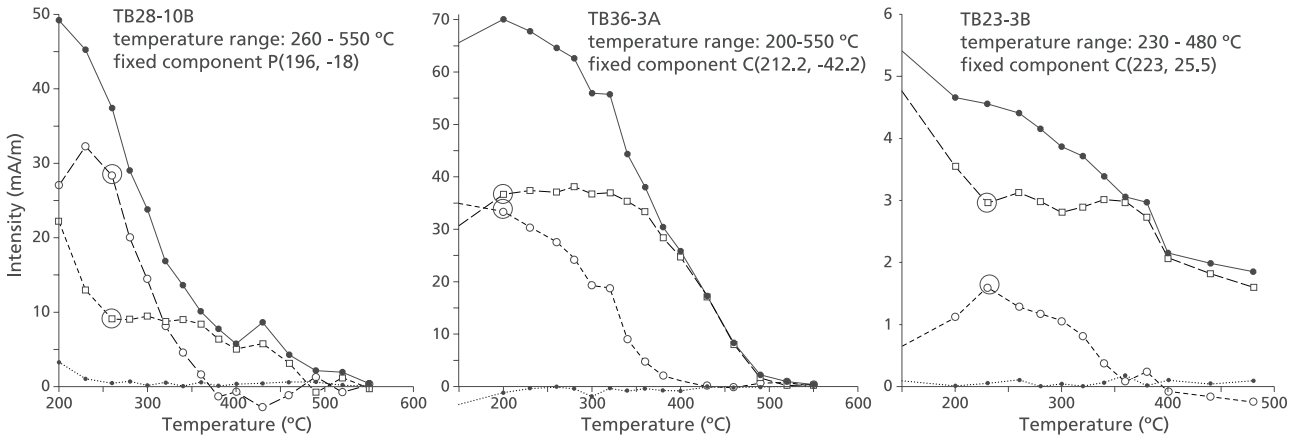

Figure 5. Remanence decay curves. The separated decay curves of the P component (dashed line, circles) and C component (dashed line, squares) are computed with PALDKPRO. Solid line shows total intensity decay. Stippled lines denote the residuals, i.e., the perpendicular distance between measured remanence vectors and the plane through the computed P and C remanence vectors. Circles show the initial intensity for different components, as used to determine the relative intensity factor (R_i).

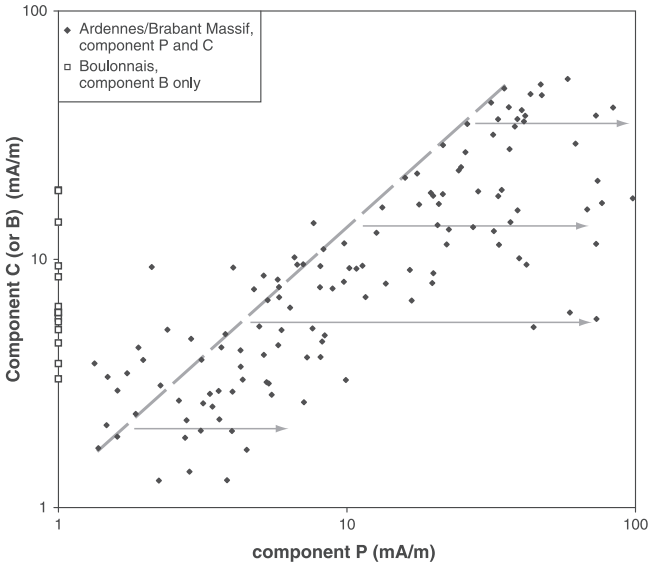

Figure 6. Initial NRM intensities (after removal of the VRM part of the NRM) for components P and C, measured for specimens from the Ardennes and Brabant Massif, plotted against each other in log-log space, and for single component B in specimen from the Boulonnais area, only indicated on the *y* axis. The dashed line indicates an approximately linear trend, arrows indicate the deviation from this lineair trend by higher component P intensities. Component B intensities are in the lower range of component P and C intensities.

Garza and Zijderveld [1996]. We refer to it as the P component. At higher temperatures up to 520°C, the other NRM component is removed that has variable in situ orientations (Figures 3a–3d). It is referred to as C component. In large parts of the Ardennes and Brabant Massif domains this C component is prefolding as discussed by *Molina Garza and Zijderveld* [1996]. In the southernmost sites of the Ardennes domain, however, this component was acquired after folding (Figures 3 and 4). The specimens from the Boulonnais area show a distinctly different demagnetization behavior. Apart from the VRM, there is only one component with highest unblocking temperatures of 430–580°C (Figure 3f). This B component has a south-southwesterly declinations and positive in situ inclinations. A fold test was not possible in the Boulonnais area and therefore it is not possible to assess whether the B component was acquired before or after tilting. The B direction is consistent with remanence directions found by *Márton et al.* [2000].

4.2. Relative Intensity of NRM Components

[16] The vectorial decomposition of the total NRM decay curve into separate decay curves for each component was used to study the pattern of initial intensity and decay characteristics for the individual components. For the Ardennes and Brabant Massif domains, the initial intensity of the P component is defined as the NRM intensity after demagnetization of the present-day field VRM component, i.e., at ~230°C. As a rule, from this temperature up, the NRM is composed of only the P and C components, as indicated by near-zero residuals in the decay plots (Figure 5). The initial NRM intensities (after decay of the VRM component) are plotted for different components in Figure 6. Maximum initial NRM intensities range from 100 mA/m for component P to 55 mA/m for component C. The initial intensities of P and C components define an approximately linear trend in a log-log plot. However, component P values deviate from a strictly linear relation, plotting to the right of the dashed line in Figure 6, at higher intensities. Conceptually, a linear relationship may be expected if components P and C were formed by the same process. The deviation of component P to higher intensities can be taken as an indication that P formed by addition of magnetic carriers. For comparison, the initial intensity of single component B from the Boulonnais domain is plotted in the same figure. The maximum initial intensities of component B, 20 mA/m, are typically lower than those for components P and C.

[17] To test whether the P component is geographically associated with the MVT ore districts, we examine the geographic variation of the initial intensity of component P with respect to component C. For all specimens the ratio of initial intensity of component P over C shows an approximately lognormal distribution. For further analysis we used the natural logarithm of the intensity ratio, resulting in the relative intensity factor $R_i = \ln (I_p/I_c)$. A histogram of R_i factors for all specimens is shown in Figure 7. The site-mean R_i factors, as well as their standard deviations, are given in Table 1. The standard deviation of the R_i factor within one site is typically small compared to the total R_i variation in all specimen from all sites. This suggests that the between-site variation in R_i factor is geologically significant.

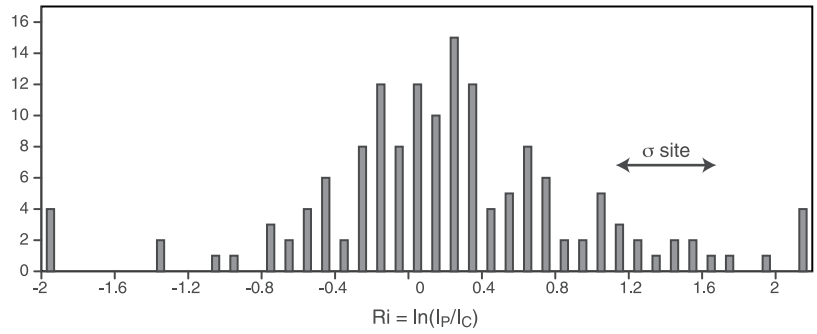

Figure 7. Histogram of relative intensity factor ($R_i = \ln(I_P/I_C)$) for all specimens (N = 158) for which the separate component P and C remanence decay curves could be determined. The typical within-site standard deviation per site (see Table 1) is indicated for comparison with the total variation in R_i.

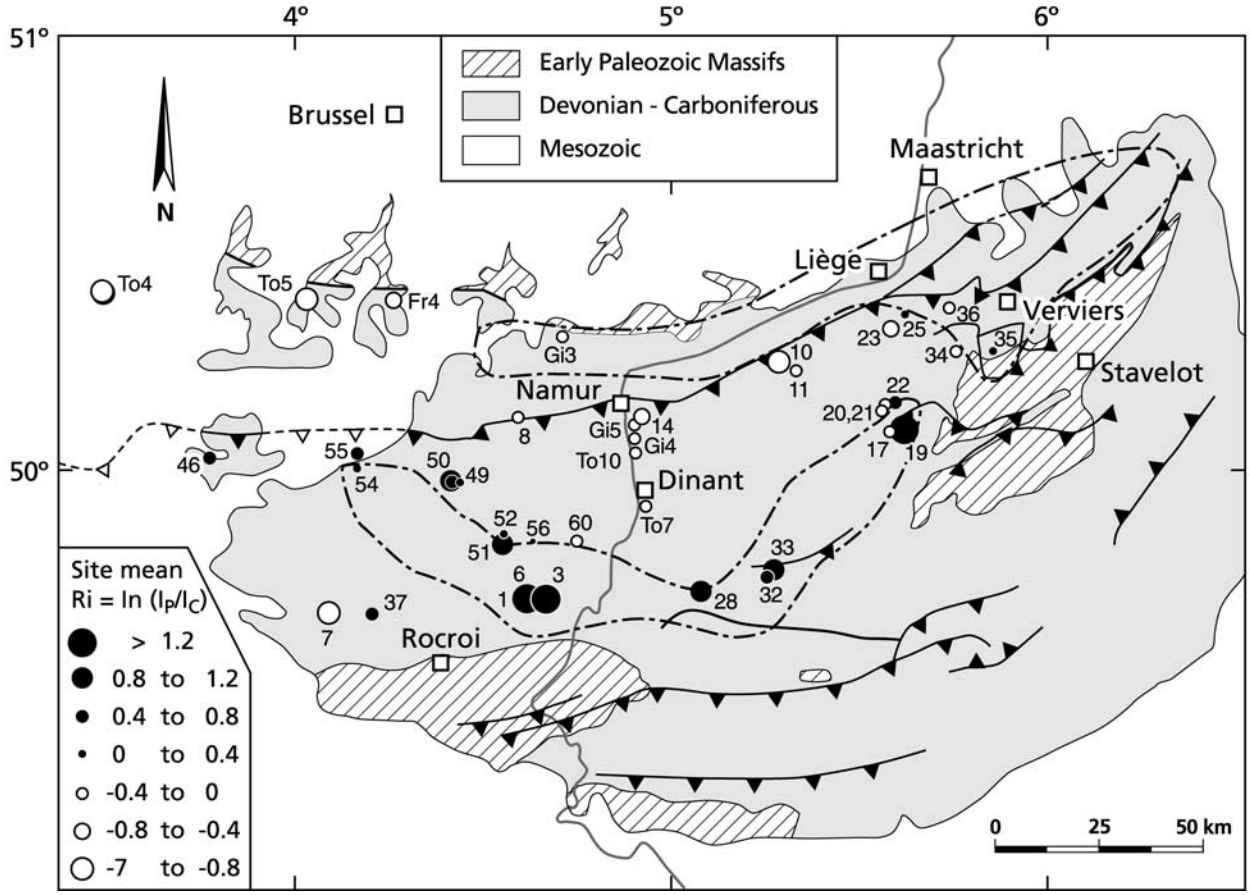

Figure 8. Simplified geological map of the Ardennes and Brabant Massif showing the geographical variation in R_i. Highest R_i values, i.e., relatively strong contributions of component P, occur in the southern part of the Ardennes, and correlate with the Dinant district of barite bearing Mississippi Valley-type (MVT) ore deposits. High R_i values do not correlate spatially with the northern MVT district, nor with proximity to major thrust faults such as the Midi Fault.

[18] Figure 8 shows the geographic variation in R_i factor. The highest values of R_i, indicating a relatively strong contribution of the P component, occur in a zone that is geographically associated with the southern MVT ore district. R_i factors are close to zero in the northeastern part of the study area, where the volumetrically more important northern MVT ore deposits occur. Strongly negative R_i factors occur in the westernmost parts of the Brabant Massif and Ardennes domains, indicating a very minor contribution of the P component. In the Boulonnais domain neither P nor C component occur and the R_i factor is not defined.

4.3. Rock Magnetic Results

4.3.1. NRM Unblocking Temperatures

[19] The separate decay curves for each component, such as shown in Figure 5, were used to analyze the maximum unblocking temperatures of the various components. Component P typically shows a rapid intensity decay in the 300 to 350°C range, but the intensity tails off to temperatures of 450°C. As a measure of the maximum unblocking temperature of component P we determined the maximum first derivative of the decay curve, i.e., the temperature at which the fastest intensity decay occurred. In Figures 5a–5c this is 320°C, 340°C, and 340°C respectively. These temperatures are shown as a histogram in Figure 9. Maximum unblocking temperatures of component P are in the range of 280 to 380°C, with a peak at 320°C. This range of maximum unblocking temperatures points to the magnetic iron sulfide, pyrrhotite, as the magnetic carrier. Measurement of the low-field magnetic susceptibility during thermal demagnetization did not show a marked decrease between 200 and 300°C [cf. *Torii et al.*, 1996], so the presence of greigite is unlikely. Also the paleotemperature conditions of the rocks do not favor greigite formation. Components C and B show maximum unblocking temperatures that range from 400 to 580°C, with typical maximum unblocking temperatures of 500 to 520°C. These maximum unblocking temperatures point to magnetite as the magnetic carrier of both components C and B.

4.3.2. Thermal Demagnetization of ARM and IRM

[20] Thermal demagnetization after ARM acquisition for 15 specimens (Figure 10) shows maximum unblocking temperatures of ~500°C. Some specimens (TB1-5, TB3-1) with a very high R_i ratio, show a comparatively rapid decay between 240 and 400°C, with steepest decay at 320–340°C. Thermal demagnetization of three orthogonal (3-D) IRMs for 15 specimens at 80 mT, 350 mT and 2 T for some typical samples are shown in Figure 11. The 3-D IRM values were chosen to best separate the contributions of magnetite, pyrrhotite and high coercivity minerals such as hematite.

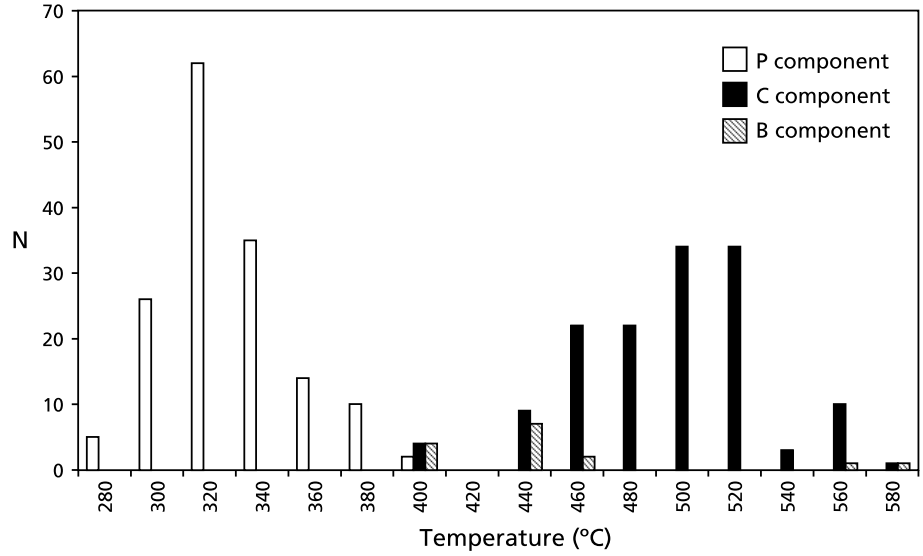

Figure 9. Maximum unblocking temperatures for components B, C, and P. For component P the temperature at which fastest decay occurs (first derivative of decay curve) is used; for components C and B the maximum unblocking temperature is indicated in the histogram (see text for discussion).

The 80 mT component invariably has the highest intensity, followed by the 350 mT component. The 2 T component only shows an important contribution in specimens that contain hematite, which are not considered in this study. The 80 and 350 mT components are both dominated by magnetite with unblocking temperatures of 500–520°C. However, in the 350 mT and 2 T components the decay is more pronounced at 320–340°C than in other temperature ranges, indicative of pyrrhotite.

4.3.3. Thermomagnetic Runs

[21] To distinguish between Curie temperatures and chemical alterations, five samples with high intensities were heated and cooled on the Curie balance in three cycles: heated to 380°C and cooled to 200°C, then heated to 500°C and cooled to 250°C, and finally heated to 700°C and cooled to room temperature. Most samples typically show the pattern in Figure 12a: a weak, but well measurable signal with a small ferromagnetic contribution compared to the paramagnetic and diamagnetic contribution. The thermomagnetic behavior is reversible up to ~400°C, as evidenced from the cooling segment back to 200°C. An unambiguous pyrrhotite Curie point is not visible in the heating run of most samples, probably due to the dominance of magnetite and the low ferromagnetic signal of rocks. At ~420°C, the magnetization increases sharply because of the formation of new magnetite, presumably from the oxidation of pyrite in air that is known to occur in the temperature range of 420 to 500°C. This is consistent with the frequent occurrence of small amounts of spurious remanences during thermal demagnetization at temperatures above 400°C. As

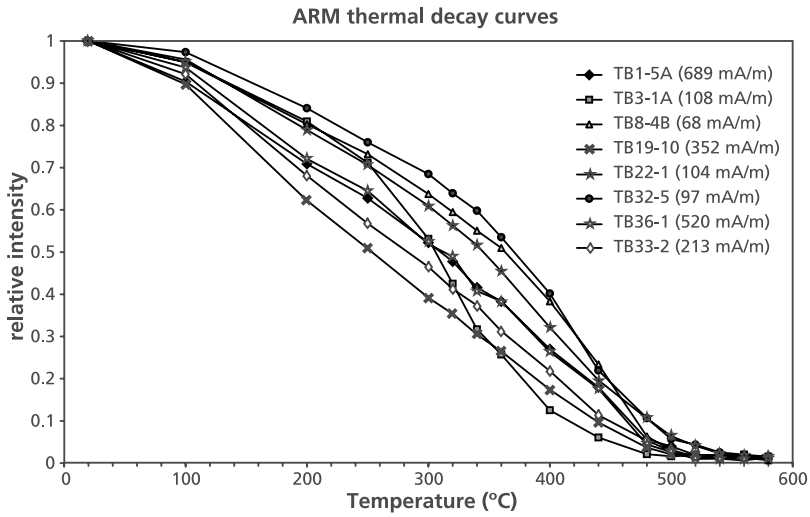

Figure 10. Thermal demagnetization decay curves after ARM acquisition to 300 mT. The intensity before thermal demagnetization is indicated in parentheses for each sample number. Maximum unblocking temperatures are 500–520°C for most samples, indicative of magnetite, but TB3-1A shows more rapid unblocking at temperatures between 200 and 400°C, suggesting the presence of pyrrhotite.

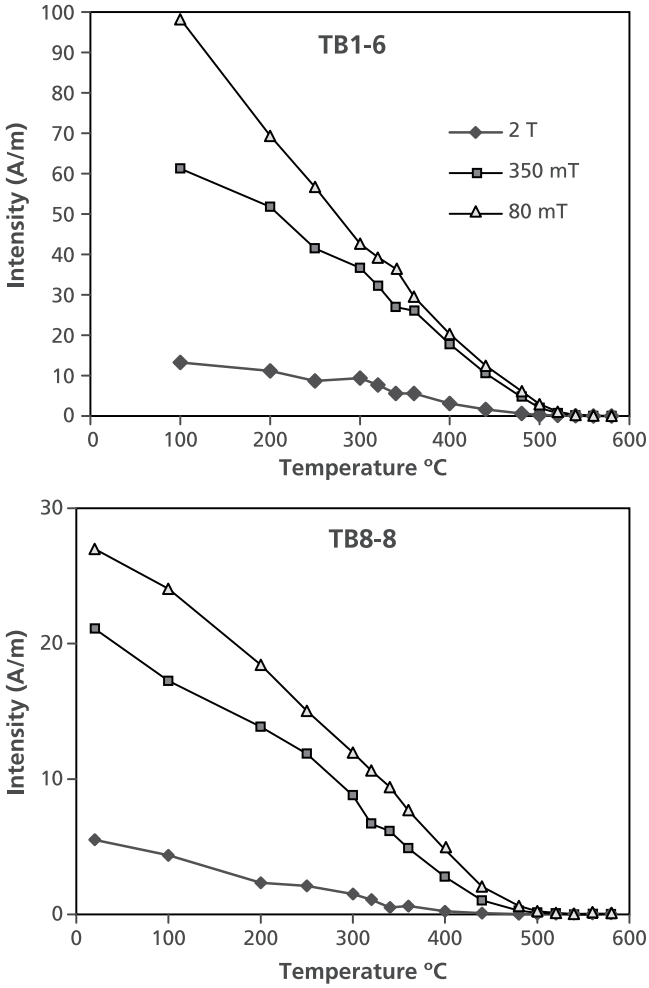

Figure 11. Intensity decay curves of thermal demagnetization of 3-D IRM. The hardest component (2 T) is all but absent in the Givetian limestone samples. The 350 and 80 mT components are both dominated by magnetite, but the 350 mT component shows a more rapid decay at 320–350°C, suggesting pyrrhotite.

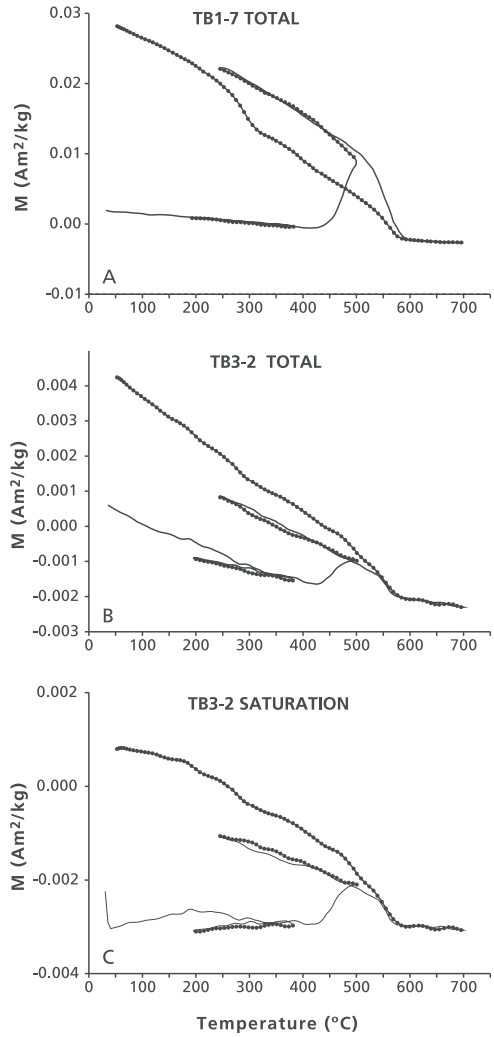

Figure 12. Thermomagnetic analyses of bulk samples performed with an improved horizontal translation Curie balance [*Mullender et al.*, 1993]. Heating rates were 10°C/min, cooling rates were 15°C/min, and the magnetic field was cycled between 100 and 300 mT. Heating (cooling) segments are indicated with solid (dotted) lines. The total magnetization shown in Figures 12a and 12b is equivalent to a conventional Curie balance signal. Sample TB1-7 (Figure 12a) is representative of most Givetian limestones from the Ardennes. The ferromagnetic signal is dominated by magnetite, a pyrrhotite Curie point is not visible in the heating run. The magnetization increases sharply at about 420°C, due to formation of new magnetite. Sample TB3-2 (Figure 12b) was collected from a Couvinian limestone next to a barite vein. The sample contains very little magnetite and the total magnetization is low. The signal can be separated into a ferromagnetic contribution (Figure 12c) and a paramagnetic/diamagnetic component contribution (not shown here). Saturation is probably not achieved at temperatures lower than 200°C, resulting in overcorrection. The ferromagnetic heating curve shows an irreversible decay up to temperatures of 350°C, indicative of pyrrhotite.

anticipated, all magnetization is lost at the Curie temperature of magnetite 580°C. The cooling segment from 500°C back to 250°C is reversible. The cooling run from 700°C lies below the 500°C heating/cooling run, indicating that part of the newly produced magnetite oxidized further to presumably hematite, with a much lower magnetization, at temperatures between 500 and 700°C. The cooling run from 700°C shows a small bend at 420°C and a distinct bend at 320°C. The meaning of the former is unclear; the latter indicates the presence of pyrrhotite. The Curie point of pyrrhotite is not detectable in the cooling run that starts from 500°C, indicating that pyrrhotite is produced from pyrite during the 500–700°C temperature interval.

[22] To visualize the contribution of pyrrhotite we ran a sample (TB3-2, Figure 12b) taken from a Couvinian limestone next to a barite vein in the southern MVT district. The specimen from this site showed a weak NRM with only the P component (Figure 3e), so its R_i value is maximal. The magnetization is dominated by the paramagnetic plus diamagnetic component with only a very small ferromagnetic part. During the first heating-cooling cycle, heating up to

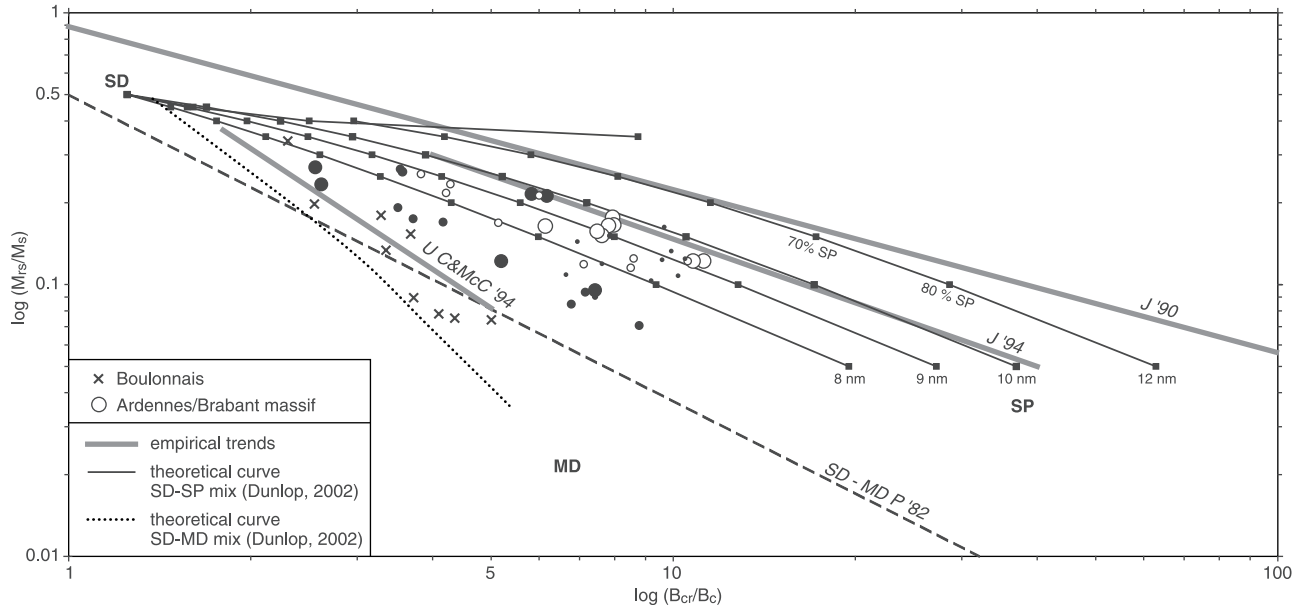

Figure 13. Hysteresis properties of samples from the Ardennes, Brabant Massif, and Boulonnais area, ratios plotted according to *Day et al.* [1977]. Different empirical trends are shown for unremagnetized (U C&McC'94) and remagnetized limestones (R J'90 and R C&McC'94) [*Jackson*, 1990; *Channel and McCabe*, 1994], mixtures of hematite and magnetite (HM C&McC'94), and mixtures of single domain and multidomain magnetite (SD-MD P'82) [*Parry*, 1982]. Theoretical mixing curves for SD-MD mixes, and SD-SP with different SP grain sizes, are shown following *Dunlop* [2002]. Samples from the Boulonnais area (crosses) fall on the unremagnetized limestone trend. Samples from the Ardennes and Brabant Massif follow the remagnetized limestone trend but shift toward lower magnetization and coercivity ratios with increasing R_i factor (symbols as in Figure 8), consistent with increasing influence of pyrrhotite in a magnetite-pyrrhotite mixture.

380°C and cooling to 200°C, a noticable irreversibility occurs. Calculation of the ferromagnetic part of the signal (Figure 12c) indicates that the irreversibility is related to a ferromagnetic contribution. This magnetic behavior is difficult to explain because chemical alteration at these temperatures is unlikely so that the observed behavior must be caused by magnetic phenomena. The maximum field used may not have been sufficient to saturate fine-grained pyrrhotite. This could be the reason for the initial increase in magnetization with temperature during the first heating run. *de Boer and Dekkers* [1998] described similar thermomagnetic behavior for hematite. The reason for the irreversibility during cooling from 380°C is unclear; possibly a harder pyrrhotite variety with a different superstructure is formed as a result of heating. Alternatively, minute amounts of oxygen may be incorporated into the pyrrhotite structure [*Graham et al.*, 1987], which yields dramatically varying thermomagnetic behavior. However, at these relatively low temperatures these phenomena are not expected to be important. A third possibility may be that the pyrrhotite oxidizes slightly. The first pyrrhotite phase that would result, the so-called anomalous pyrrhotite [*Taylor*, 1971] is a nonmagnetic pyrrhotite variety. Which process operates remains speculative at this stage. As in the other samples upon heating above 420°C, magnetite is produced as well as "classic" pyrrhotite at temperatures between 500 and 700°C.

4.3.4. Hysteresis Measurements

[23] Figure 13 shows hysteresis parameters for a range of samples from the Ardennes, Brabant Massif and Boulonnais domains plotted on a Day plot [*Day et al.*, 1977], plotting the saturation remanence (M_r) to saturation magnetization (M_s) ratio against the coercivity of remanence (B_{cr}) to coercive field (B_c) ratio. There is a clear difference in hysteresis properties between samples from the Boulonnais domain on the one hand and those from Ardennes and Brabant Massif domains on the other. The magnetite-dominated Boulonnais samples are consistent with the trend for unremagnetized Maiolica limestones as defined by *Channel and McCabe* [1994]. They straddle the single-domain-multidomain (SD-MD) mixing line derived on theoretical grounds by *Dunlop* [2002]. The samples from the Ardennes and Brabant Massif domains are characterized by wasp-waisted hysteresis loops and plot close to the trend for remagnetized limestones from North America and the Craven Basin defined by *Channel and McCabe* [1994]. They also plot slightly to the left of the trend. Both modeling of synthetic hysteresis loops by *Tauxe et al.* [1996] and theoretical mixing curves calculated by *Dunlop* [2002] indicate that the remagnetized limestone trend is likely the result of a mixture of SD and SP magnetite. According to the SP-SD mixing interpretation the samples from the Ardennes and Brabant Massif domains would plot on the 40–80 vol % super paramagnetic (SP) grains, indicating that the SP contribution is large in these samples.

[24] The R_i ratio of the Ardennes and Brabant Massif samples generally increases toward the left in the Day plot. Such a trend may be explained by a decrease in SP grain size (see Figure 13) or by the contribution of pyrrhotite. As illustrated by *Peters and Dekkers* [2003] hysteresis properties of pyrrhotite occupy a field with lower coercivity ratios

compared to magnetite. A mixture of magnetite and pyrrhotite would therefore pull the hysteresis properties to the left in the Day plot.

5. Discussion

5.1. NRM Components

[25] There is no doubt that the two NRM components that occur in the Ardennes and Brabant Massif are remagnetized components. The P component is postfolding in all cases and consistent with an early Permian position on the APWP for Baltica [*Molina Garza and Zijderveld*, 1996]. The C component is prefolding in the northern part of the Ardennes, and postfolding in the southern parts. A similar diachronous relation between remagnetization and folding was found in the NE Rhenisch Massif, the eastward extension of the Ardennes fold belt into Germany [*Zwing et al.*, 2002]. The C component is consistent with a Late Carboniferous position on the APWP for Baltica [*Molina Garza and Zijderveld*, 1996; *Zwing et al.*, 2002].

[26] The nature and time of acquisition of the B component in the Boulonnais area is not clear. The in situ orientation is consistent with the orientation of the C component in the Ardennes. Therefore the B component may be interpreted as a posttilting remagnetization, acquired during the Late Carboniferous as suggested by *Márton et al.* [2000]. However, the Boulonnais sites are on the northern side of the Midi Fault, and therefore occupy a northerly position in the Variscan orogenic belt. It is unlikely therefore that the B component represents a postfolding equivalent of C in the Boulonnais area. The orientation of the B component is inconsistent with the orientation of the P component in the Ardennes. The B component is interpreted therefore as a third NRM component, and not as the equivalent of either the P or C components.

[27] Moreover, hysteresis properties of the Boulonnais samples fall on the unremagnetized trend, close to the SD-MD mixing line, whereas the Ardennes and Brabant Massif samples fall on either the remagnetized limestone trend or the SD-SP mixing envelope. Therefore we have to consider the possibility that the B component is not a remagnetization, but rather a primary component. The primary nature of component B would imply that the Middle Devonian paleolatitude of the Boulonnais was about 5° north of the equator. Paleogeographically (Figure 14), Baltica, coming from a position just south of the equator in the Silurian, would have moved across the equator to the north in the Devonian during the opening of the Rheic ocean to the south and the development of the Rhenohercynian sedimentary basin in the Devonian and Early Carboniferous. In the Carboniferous Baltica would move back to the southern hemisphere during the closing of the Rheic ocean and Variscan orogeny in the middle to Late Carboniferous. After closure of the Rheic ocean Baltica and Gondwana continued their northward drift. Geologically, this is not an unrealistic scenario (Figure 14).

[28] There is an almost complete lack of reliable paleomagnetic data for Baltica for the Middle Devonian to Late Carboniferous [*Torsvik et al.*, 1996]. Therefore a possible primary middle Devonian NRM component in the Boulonnais area would be an important addition to the paleomagnetic data set for Baltica.

5.2. Magnetic Carriers and Granulometry

[29] To understand the remagnetization process that produced the various components in the Ardennes and Brabant Massif, it is essential to constrain the mineralogy and grain size of the magnetic carriers for each magnetic component. As indicated by the highest unblocking temperatures of NRM, ARM, 3-D IRM, thermomagnetic analysis and hysteresis measurements, the dominant magnetic carrier in all samples is magnetite. Magnetite is responsible for both components C and B. However, the highest unblocking temperatures are typically 520°C, considerably lower than the Curie temperature of SD magnetite. Hysteresis measurements indicate that C component magnetite in the Ardennes and Brabant Massif is a mixture of SD and SP magnetite but the precise grain size distribution is not clear. Taken at face value, the mixing lines by *Dunlop* [2002] (Figure 13) suggest that the Ardennes and Brabant Massif samples contain a bimodal grain size distribution of small SD grains (30 nm) and 8–10 nm SP grains in volume proportions varying from 40 up to 80% SP. The SP grains, characteristic of remagnetized limestones, do not contribute to the NRM but have a large influence on the hysteresis properties. The small SD grains carry the NRM and their small grain size results in the typical low unblocking temperatures of 520°C. However, such a bimodal distribution may not be geologically realistic.

[30] There are two factors that have not been taken into account in the theoretical mixing curves by *Dunlop* [2002] that may play a role, particularly for the larger SP grains. These are non-Langevin behavior as a result of anisotropy energy and thermal activation. *Tauxe et al.* [1996] did incorporate the non-Langevin behavior of larger SP grains in their modeling of synthetic hysteresis curves. The net result of these two factors is such that a mix of larger SP grains and SD grains, i.e., a single distribution of grain sizes straddling the SP-SD threshold size, will result in similar trends in the Day plot as a bimodal mix of SD and 8–10 nm SP grains. *Tauxe et al.* [1996] found that the remagnetized limestone trend of *Channel and McCabe* [1994] could best be simulated by such a single grain size distribution straddling a SP/SD threshold size of 15 nm, which is markedly smaller than the SP/SD threshold size used by *Dunlop* [2002] of 30 nm. For most geological situations of crystallization and authigenic grain growth, the most plausible grain-size distribution is a lognormal distribution. The majority of the magnetite grains in the remagnetized Devonian limestones would then be large SP grains with a relatively small proportion of grains in the SD range.

[31] The hysteresis properties of the B component indicate magnetite of single to pseudo single domain (PSD) grain size (larger than about 100 nm) for which an unblocking temperature of 580°C would be expected. The maximum unblocking temperatures of the Boulonnais samples vary, but are generally lower than 580°C. It is not clear what may cause this reduction in unblocking temperatures, assuming that magnetic carriers are indeed PSD magnetite. One possible explanation is a titanomagnetite component in the detrital magnetite. However, this remains to be confirmed.

[32] The P component NRM shows highest unblocking temperatures of typically 320 to 340°C, but in some cases up to 380°C. Thermal decay curves of ARM and IRM show

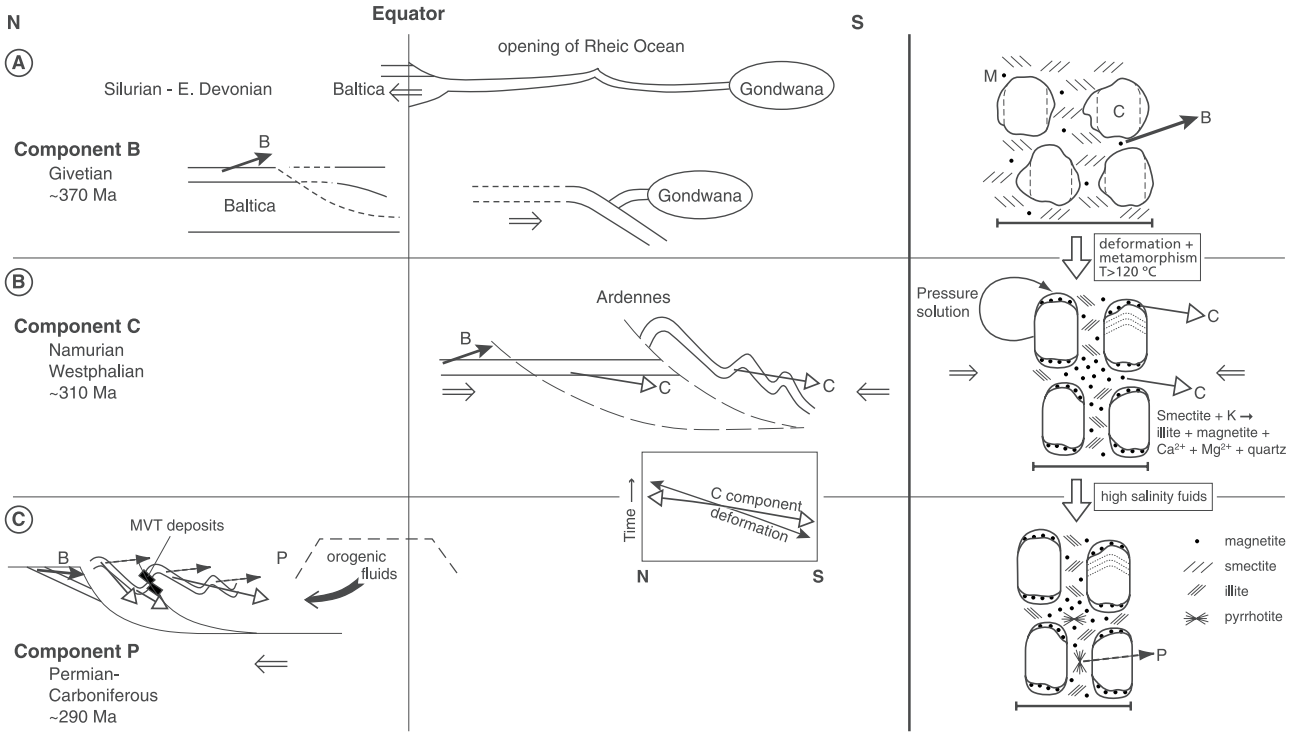

Figure 14. Conceptual model showing the relation between deformation, fluids and remagnetization on a regional geological scale and on grain-size scale. (a) Deposition of Givetian limestone at the passive northern margin of the Rheic Ocean between Baltica and Gondwana. Primary component B is acquired, indicating a paleogeographic position of the Boulonnais area, as part of Baltica, at about 5° north of the equator. During the Late Devonian to Early Carboniferous the Rheic Ocean closes by southward drift of Baltica as a result of southward subduction of oceanic crust. Schematic microtexture shows carbonate grains surrounded by smectite containing clay with trace amounts of magnetite. (b) Closure of the Ardennes Basin by progression of the Variscan deformation front from south to north during the Carboniferous. The Variscan orogeny is the result of closure of the Rheic Ocean and collision of Baltica and Gondwana. The Ardennes area is situated a few degrees south of the equator. On a microscale, pressure solution processes result in dissolution of carbonate on stressed surfaces and precipitation of carbonate on free surfaces. Simultaneously, smectite converts to illite, releasing Fe^{2+} that remains in clay aggregates as fine grained (10–30 nm) magnetite or as precipitates on growing carbonate surfaces. The newly formed magnetite carries NRM component C. Mg^{2+} released during smectite to illite conversion, results in precipitation of dolomite. All processes take place in the presence of internal hostrock buffered fluids. (c) Orogenic fluids percolate through the foreland fold-and-thrust belt of the Ardennes, and result in MVT Pb-Zn ore deposits during the Late Carboniferous and Early Permian. The Ardennes and Brabant Massif are now again situated slightly north of the equator. Pyrrhotite is formed as a result of interaction between these high salinity fluids and carbonates. Iron may have been present as pyrite or magnetite, or may have been introduced with the fluid. The newly formed pyrrhotite aquires the NRM component P.

more rapid decay at 320 to 340°C. A similar rapid decay is visible in thermomagnetic runs on samples that only exhibit the P component, not the C component. This suggests the presence of iron sulfide as the carrier of the P component. *Robion et al.* [1997] clearly demonstrated the presence of pyrrhotite in, and to the south, of the Rocroi Massif. Although pyrrhotite is unequivocally detected through it s34 K magnetic transition by *Robion et al.* [1997], their samples show highest unblocking temperatures in the temperature range 350–370°C. Such high unblocking temperatures have also been described by *Rochette et al.* [1990] for pyrrhotite. This is similar to the unblocking temperature range that we find for the P component. These unblocking temperatures above the Curie temperature for monoclinic pyrrhotite (320°C), suggest that iron sulfide found in this and other studies of sedimentary rocks does not behave as ideal monoclinic pyrrhotite, possibly as a result of small amounts of oxygen in the crystal lattice [*Graham et al.*, 1987]. Hysteresis properties of samples from the Ardennes and Brabant Massif are consistent with a mix of SP-SD magnetite (C component) and pyrrhotite (P component) and, with increasing P component intensity (R_i factor), the hysteresis measurements plot toward lower B_{cr}/B_c values, as would be expected on the basis of pyrrhotite hysteresis properties [*Peters and Dekkers*, 2003].

5.3. Remagnetization Mechanisms

[33] We will now discuss possible scenarios for remagnetization mechanisms for the C and P components based on an integration of rock and paleomagnetic results and on

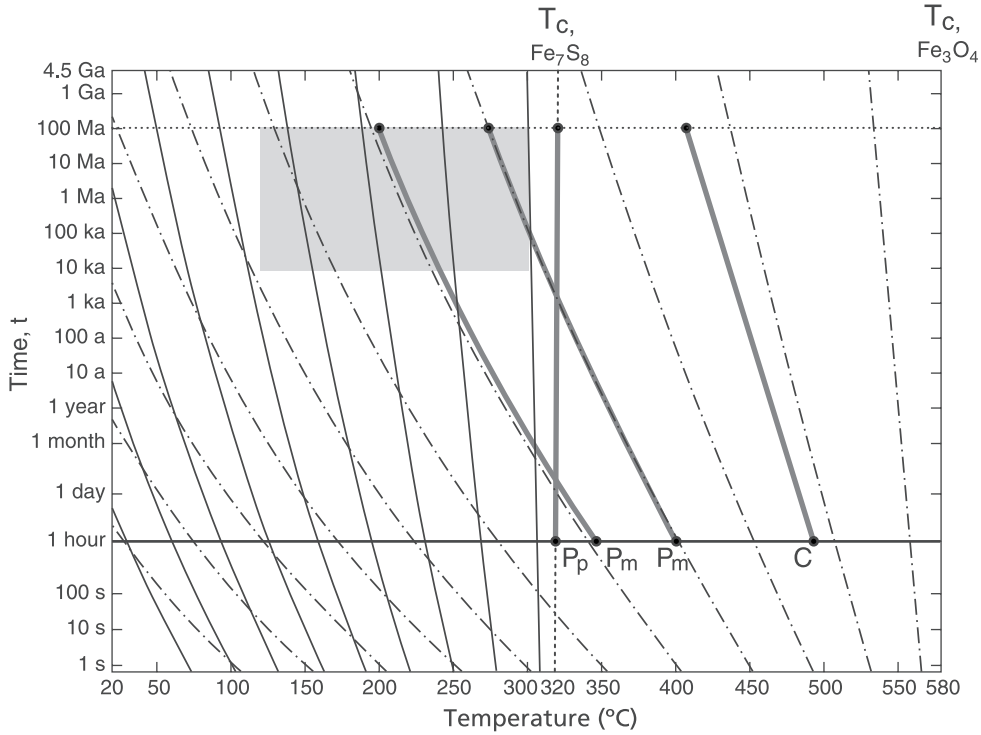

Figure 15. Time versus temperature contours for pyrrhotite (steep solid lines) and magnetite (dashed lines) after *Dunlop et al.* [2000]. Maximum unblocking temperatures for components P and C are shown for a thermal demagnetization period of 1 hour. The shaded square indicates temperatures that may have been reached in the Ardennes and Brabant Massif. Metamorphism due to Variscan orogenesis (120–310°C) in the Carboniferous may have lasted tens of millions of years. Local heating up to 300°C, due to percolation of hot MVT fluids in the Late Carboniferous to Early Permian, would have lasted for short periods (<10 Myr). Component C cannot have been the result of partial TVRM. The unblocking temperatures between 350 and 400°C of component P, i.e., the low intensity tail in the decay curve, may be caused locally by TVRM of preexisting magnetite (P_m contours). Component P pyrrhotite (P_p) cannot be the result of TVRM but must be by local hydrothermal heating.

spatial and temporal correlations with geological processes. First we need to consider whether the C and P component could be the result of partial TVRM (thermoviscous remanent magnetization). In the Ardennes and Brabant Massif the maximum paleotemperature reached during Variscan deformation varies from 120 to 310°C [*Fielitz and Mansy*, 1999] (Figure 1). These temperatures are too low to explain maximum unblocking temperatures in magnetite of ~520°C by a TVRM mechanism for component C (Figure 15).

[34] For component P the reasoning is more complex. The P component was acquired after Variscan deformation and metamorphism in the Late Carboniferous to Early Permian (Figure 2). At that time regional paleotemperatures were between 120 and 200°C with higher temperatures up to 310°C next to faults that acted as conduits for hot fluids [*Schroyen*, 2000]. Although our rock magnetic results indicate that component P is carried by pyrrhotite, we consider the possibility that component P is solely or partly the result of a partial TVRM of preexisting magnetite. A paleotemperature of 120°C is not sufficient to produce a TVRM in magnetite with unblocking temperatures of 350°C. However, the locally occurring paleotemperatures of 300°C would be sufficiently high to produce a TVRM. Therefore in restricted areas next to major faults, partial TVRM of preexisting magnetite may play a subsidiary role as a magnetic carrier of the P component. Alternatively, component P may be a TVRM of pyrrhotite produced earlier, for example during the same event that resulted in magnetite formation and acquisition of component C. However, time-temperature contours (Figure 15) indicate that paleotemperatures in excess of 300°C would be required to produce a TVRM in pyrrhotite with 320°C unblocking temperatures. Such regional high temperatures were not reached after Variscan deformation, in the waning stages of orogenic activity [*Fielitz and Mansy*, 1999].

[35] Summarizing, partial TVRM as the remagnetization mechanism can be excluded for both remagnetized components on the basis that sufficiently high paleotemperatures were not reached and that maximum paleotemperatures were not reached at the time and place of remagnetization (component P). Therefore remagnetization in these limestones must have been the result of remagnetization CRM caused by the growth of a new magnetic phase through the blocking volume: i.e., small SD magnetite in the case of component C and, most likely, pyrrhotite in the case of component P.

5.3.1. C Component

[36] The timing of acquisition of component C with respect to geological processes gives important clues to possible remagnetization mechanisms. The overview in Figure 2 indicates that acquisition of component C occurred during the Variscan orogeny. Variscan folding and thrusting coin-

cides with the formation of illite from smectite, as indicated by illite K-Ar ages [*Pique et al.*, 1984]. Studies of syndeformation veins [*Muchez et al.*, 2000] suggest that low-salinity host rock buffered fluids were present at that time and were derived from the marine depositional environment. Calcium carbonate in the fluids is thought to be derived locally by pressure-solution deformation processes, as evidenced by intense stylolitisation of the carbonates. Mechanisms in which externally derived fluids are required, for example as an oxidizing agent [*Suk et al.*, 1990], in connection with hydrocarbon migration [*McCabe and Elmore*, 1989], or as mineralizing fluids [*Lewchuk and Symons*, 1995], are therefore not realistic for the C component.

[37] Component C is present in all of the Ardennes and Brabant Massif, but is absent in the Boulonnais area. The only geological factor that differs considerably between these two areas is the maximum paleotemperature, which is less than 55°C in the Boulonnais area and between 120 and 310°C in the Ardennes and Brabant Massif. This suggests that temperatures in the range 55 and 120°C were instrumental in the process that resulted in the formation of the component C CRM. One of the metamorphic reactions occurring in that temperature range that would liberate the iron required for the formation of magnetite, is the smectite to illite conversion reaction [*Katz et al.*, 1998, 2000]. Although the exact nature and conditions of smectite to illite conversion is complex and the subject of discussion [*Cuadros and Linares*, 1996], it is clear that the conversion takes place in the temperature range from 50 to 110°C [*Weibel*, 1999, and references therein]. Illite is produced from smectite via several stages of intermediate mixed layer smectite/illite. Different reaction formula are possible depending on the exact smectite composition but, in general, K^+ is consumed and Na^+, Ca^{2+}, Mg^{2+}, Fe^{2+} and SiO_2 are released (see Figure 14). Traditionally, the conversion of smectite to illite is interpreted in terms of a pretectonic diagenetic process. Highest paleotemperature values are correlated to the thickest sedimentary overburden. However, *Han et al.* [2000] suggested that not only sedimentary overburden, but also tectonic overburden from thrust sheets, may play a role in diagenesis and metamorphism of the Paleozoic sequence in the Ardennes. If our interpretation is correct and the C component is a CRM formed as a by-product of illite formation, this implies that the metamorphic event during which illite formed occurred after folding and thrusting in the south and prior to folding and thrusting in the north (Figure 14). This metamorphic event may still have been diachronous but proceeded faster from south to north than the actual folding and thrusting. *Han et al.* [2000] also shows that not all smectite was converted to illite in the Ardennes. Conversion of part of the smectite is thought to be limited by lack of K^+ and by porosity decrease as a result of early cementation. Pure limestones contain very little K^+, but it occurs in abundance in shales with more detrital components. This may explain the well-developed C component in the dark grey Givetian limestones: they contain both comparatively high amounts of clay minerals (including smectite) and the necessary K^+.

[38] In addition to fluids and to increasing temperature producing illite from smectite, a third factor may play a role. The dominant deformation mechanism at temperatures below 250°C in carbonates is most likely pressure solution [*Rutter*, 1976]. Pressure solution refers to the process in which grains dissolve at intergranular contacts and precipitate in the pore space or on free unstressed surfaces. This process results in compaction and deformation. Stylolite surfaces frequently recognized in carbonate rocks of the Ardennes are the result of such pressure solution processes. We can therefore assume that pressure solution occurred during the smectite to illite conversion reaction temperature interval. Dissolution and precipitation processes may have enhanced the availability of K^+ to produce illite from smectite. Iron released during the smectite-illite conversion would partly remain in situ in the clay aggregates, where it would crystallize as fine-grained magnetite. In that case the magnetite grain size would be determined by the diffusion distance of Fe^{2+} in clay during the smectite to illite conversion. This may result in the narrow range of SP/SD grains as inferred from the hysteresis data (10–30 nm). On the other hand, Fe^{2+} may diffuse in the fluid and precipitate on unstressed surfaces as magnetite inclusions in calcite and dolomite growth zones. SEM observations of remagnetized carbonates [*Weil and van der Voo*, 2002; *Xu et al.*, 1998] indicate that magnetite does indeed occur in clay domains, at growth interfaces of calcite and/or dolomite, and as inclusions in calcite and dolomite (see Figure 14). All these sites are consistent with magnetite crystallization as a result of smectite to illite conversion during pressure solution processes. Local dolomitization and dedolomitization are the combined consequence of pressure solution processes and Mg^{2+} release during smectite-to-illite conversion and should not be considered as an independent process responsible for remagnetization as suggested previously [*Loucks and Elmore*, 1986; *Hart and Fuller*, 1988; *Xu et al.*, 1998].

5.3.2. P Component

[39] The P component was acquired after Variscan folding in all cases. The fit to the apparent polar wander path for Baltica suggests that component P was acquired in the Late Carboniferous to Early Permian [*Molina Garza and Zijderveld*, 1996]. The P component was acquired therefore after all regional metamorphic events. The timing of acquisition of the P component overlaps with the earliest stages of MVT mineralization and may be genetically related to the MVT fluids. The intensity of component P with respect to component C is spatially correlated with the southern barite-bearing MVT mineralization district. This suggests that mineralizing fluids of a particular composition were related to P component remagnetization.

[40] Pyrrhotite has been regularly reported in MVT deposits, but is present in small amounts [*Symons et al.*, 1998; *Jochum*, 2000]. Pyrrhotite may form from magnetite or pyrite or may precipitate directly from fluids. Reducing conditions are needed to produce pyrrhotite, which contrasts with oxidizing conditions needed to produce barite. It is therefore unlikely that pyrrhotite and barite precipitated at the same time. There is no direct evidence for the age of the two Belgian MVT districts other than that ore veins crosscut Westphalian sediments in the Namur-Vervier District, and are covered by Cretaceous sediments. In a study of the direct continuation of the Variscan Belt in Germany, *Jochum* [2000], based on Rb-Sr dating and geologic relations, showed that there were several stages of MVT mineralisation ranging in age from late Variscan (Carboniferous) to Jurassic. The occurrence of pyrrhotite is restricted to the

earliest mineralisation stage, followed by deposition of siderite and Pb-Zn sulfides. According to *Jochum* [2000], thermal maturation of organic matter during the ascent of Variscan orogenic fluids led to sulfate reduction, which in turn triggered base metal sulfide precipitation. According to *Heijlen et al.* [2001], the high salinity fluids responsible for MVT mineralization, were generated as formational fluids during the formation of Givetian evaporites found in drill holes in the southern Ardennes. They suggest that these fluids may have caused dolomitization in the Early Carboniferous, and subsequently remained deeply buried during Variscan deformation. The fluids were expelled in the Mesozoic, possibly during extension, resulting in MVT mineralisation.

[41] Faults are generally regarded as highly permeable conduits for fluids. This may result in chemical alteration of rocks close to faults and to temperature effects due to the relatively high temperature of the fluids. The temperature effects of fluid migration were summarized by *Schroyen* [2000]. Drill core data show that paleotemperature anomalies are associated with major thrust faults. Paleotemperatures of 310°C were recorded close to the Midi Fault, against a background temperature of 150–190°C. *Lünenschloss et al.* [1997] modeled this temperature anomaly as the result of advective heat transport by hot fluids that preferentially migrate along faults. It is interesting therefore to note that the intensity of component P does not appear to be correlated to proximity to major faults. In addition, the lack of correlation between the intensity and highest unblocking temperature of component P with the maximum paleotemperature indicates that temperature was not the controlling factor in the acquisition of component P. An external fluid of particular composition, possibly in combination with organic matter along the fluid pathway, seems to have been instrumental in the remagnetization process of the P component. The pervasive nature of the P component in Givetian limestones suggests that these limestones were permeable. Permeability may have been enhanced by dolomitization and fracturing.

6. Conclusions

[42] By integrating detailed geological information on deformation, paleotemperatures and the occurrence of MVT ore deposits with paleomagnetic and rock magnetic results, we tested different remagnetization mechanisms for the Devonian limestones in the Ardennes and Brabant Massif. The two remagnetized NRM components, the Carboniferous C and Late Carboniferous to Early Permian P, are produced by two different mechanisms. Component C, carried by magnetite in the SP to small SD grain size range (10–30 nm), is most likely formed as a by-product of the conversion of the clay mineral smectite to illite [*Katz et al.*, 1998], which takes place at temperatures of about 110°C. Illite was formed during Variscan deformation. The smectite-to-illite reaction and the diffusion of Fe^{2+} to the site of precipitation of magnetite are likely to have been enhanced by pressure solution deformation processes. This simultaneously explains the microscopic observation in remagnetized limestones that fine-grained magnetite is sited in both clay domains and as inclusions in growth zones of calcite/dolomite [*Weil and van der Voo*, 2002; *Xu et al.*, 1998], and the ubiquitous occurrence of remagnetization simultaneous with orogenic deformation.

[43] The only area that potentially preserves a primary Middle Devonian NRM component is the Boulonnais area in northwestern France. Paleotemperatures in this area did not exceed 55°C, preventing the smectite-illite conversion from taking place. On the basis of the hysteresis properties and on the geologically consistent paleogeography, the preferred interpretation is that the B component is a primary component of Givetian age.

[44] Component P most likely resides in pyrrhotite. Component P occurs pervasively in the Ardennes and Brabant Massif, but its intensity is spatially correlated with the southern, barite-bearing MVT district. The timing and spatial intensity variation both suggest that pyrrhotite crystallization was a result of the circulation of external, high salinity fluids. Percolation of these fluids through organic matter contained in Devonian and Carboniferous units may have produced the reducing conditions necessary for precipitation of pyrrhotite. Pyrrhotite could be the product of reduction of magnetite or pyrite, or may have precipitated directly from the fluid. Locally, where higher temperatures were reached at that time (300°C) as a result of heat advection by hot fluids, a partial TVRM of preexisting magnetite may contribute to component P.

[45] Remagnetization processes in the Ardennes and Brabant Massif were controlled by the following factors: (1) Increase in temperature, potentially to produce a partial TVRM, but more importantly as a condition for the smectite-illite reaction to take place. (2) Deformation or compaction, resulting in pressure solution processes enhancing the smectite-illite conversion by dissolution and precipitation reactions of surrounding carbonates. (3) Fluids, internal as a medium for pressure solution processes and for diffusion of Fe^{2+}, or external hydrothermal flow, resulting in authigenesis of pyrrhotite.

[46] The remagnetization mechanism of component C, producing the typical remagnetized trend in the Day plot, is expected to be all but ubiquitous in limestones sampled in or close to orogenic belts. The required conditions for smectite-to-illite conversion, temperatures in excess of 110°C and enhanced by pressure solution processes during compaction and/or deformation, are indeed the rule rather than the exception for such limestones. Remagnetization as a result of authigenesis of magnetic minerals by the circulation of external fluids is likely to be geographically more restricted. Because remagnetizations in limestones can be produced by different mechanisms, caution is called for when using the timing of remagnetization to date a geological event. In the Ardennes, the MVT deposits in the southern Dinant district are likely to be of Late Carboniferous to Early Permian age.

[47] **Acknowledgments.** We thank Jan Kees Blom, Cor de Boer, Tom Mullender, Piet Jan Verplak, and Henk Meijer, for their help in sampling and laboratory support. We thank Rob van der Voo, Arlo Weil, and Cor Langereis for the discussions on this subject. We greatly appreciate the helpful reviews and comments by David Symons, Phillip Schmidt, and Tim Rolph. This study was supported by NWO-ALW. This research was supported by the Geodynamic Research School (GOI).

References

Ahrendt, H., N. Clauer, J. C. Hunziker, and K. Weber, Migration of folding and metamorphism in the Rheinisches Schiefergebirge deduced from K-Ar and Rb-Sr age determinations, in *Intracontinental Fold Belts: Case*

Studies in the Variscan Belt of Europe and the Damara Belt in Namibia, edited by H. Martin, and F. W. Eder, pp. 323–338, Springer-Verlag, New York, 1983.

Banerjee, S., R. D. Elmore, and M. H. Engel, Chemical remagnetization and burial diagenesis: Testing the hypothesis in the Pennsylvanian Belden Formation, *J. Geophys. Res.*, *102*, 24,825–24,842, 1997.

Brothers, L. A., M. H. Engel, and R. D. Elmore, A laboratory investigation of the late diagenetic conversion of pyrite to magnetite by organically complexed ferric iron, *Chem. Geol.*, *130*, 1–14, 1996.

Channel, J. E. T., and C. McCabe, Comparison of magnetic hysteresis parameters of unremagnetized and remagnetized limestones, *J. Geophys. Res.*, *99*, 4613–4623, 1994.

Cuadros, J., and J. Linares, Experimental kinetic study of the smectite-to-illite transformation, *Geochim. Cosmochim. Acta.*, *60*, 439–453, 1996.

Day, R., M. Fuller, and V. A. Schmidt, Hysteresis properties of titanomagnetites: Grain size and compositional dependence, *Phys. Earth Planet. Inter.*, *13*, 260–267, 1977.

de Boer, C. B., and M. J. Dekkers, Thermomagnetic behaviour of haematite and goethite as a function of grain size in various non-saturating magnetic fields, *Geophys. J. Int.*, *133*, 541–552, 1998.

Dejonghe, L., Zinc-lead deposits of Belgium, *Ore Geol. Rev.*, *12*, 329–354, 1998.

Delvaux, D., Structures tardi- et post Hercyniennes dans le bord sud du synclinorium de Dinant, entre Han-sur-Lesse et Beauraing (Belgique), *Ann. Soc. Geol. Belg.*, *112*, 317–325, 1990.

Dunlop, D. J., Theory and application of the Day plot (M_{rs}/M_s versus H_{cr}/H_c): 1. Theoretical curves and tests using titanomagnetite data, *J. Geophys. Res.*, *107*(B3), 2056, 10.1029/2001JB000486, 2002.

Dunlop, D. J., O. Ozdemir, D. A. Clark, and P. W. Schmidt, Time-temperature relations for the remagnetization of pyrrhotite (Fe_7S_8) and their use in estimating paleotemperatures, *Earth Planet. Sci. Lett.*, *176*, 107–116, 2000.

Elmore, R. D., D. London, D. Bagley, and D. Fruit, Remagnetization by basinal fluids: Testing the hypothesis in the Viola Limestone, southern Oklahoma, *J. Geophys. Res.*, *98*, 6237–6254, 1993.

Fielitz, W., and J. L. Mansy, Pre- and synorogenic burial metamorphism in the Ardenne and neighbouring areas (Rhenohercynian zone, central European Variscides), *Tectonophysics*, *309*, 227–256, 1999.

Graham, J., C. E. G. Bennett, and A. Riessen, Oxygen in pyrrhotite: 1. Thermomognetic behavior and annealing of pyrrhotites containing small quantities of oxygen, *Am. Mineral.*, *72*, 599–604, 1987.

Han, G., A. Preat, H. Chamley, J. F. Deconinck, and J. L. Mansy, Palaeozoic clay mineral sedimentation and diagenesis in the Dinant and Avesnes Basins (Belgium, France): Relationship with Variscan tectonism, *Sediment. Geol.*, *136*, 217–238, 2000.

Hart, M., and M. Fuller, Magnetization of a dolomite bed in the Monterey Formation: Implications for diagenesis, *Geophys. Res. Lett.*, *15*, 491–494, 1988.

Heijlen, W., P. Muchez, and D. Banks, Origin and evolution of high-salinity, Pb-Zn mineralising fluids in the Variscides of Belgium, *Miner. Deposita*, *36*, 165–176, 2001.

Helsen, S., Conodont colour alteration maps for Paleozoic strata in Belgium, northern France and westernmost Germany - preliminary results, *Ann. Soc. Géol. Belg.*, *115*, 135–143, 1992.

Horton, R. A., J. W. Geissman, and R. J. Tschauder, Paleomagnetism and rock magnetism of the Mississippian Leadville (Carbonate) Formation and implications for the age of sub-regional dolomitization, *Geophys. Res. Lett.*, *11*, 649–652, 1984.

Jackson, M., Diagenetic sources of stable remanence in remagnetized Paleozoic cratonic carbonates, *J. Geophys. Res.*, *95*, 2753–2761, 1990.

Jochum, J., Variscan and post-Variscan lead-zinc mineralization, Rhenish Massif, Germany: Evidence for sulfide precipitation via thermochemical sulfate reduction, *Miner. Deposita*, *35*, 451–464, 2000.

Jordanova, N., B. Henry, D. Jordanova, Z. Ivanov, D. Dimov, and F. Bergerat, Paleomagnetism in northwestern Bulgaria: Geological implications of widespread remagnetization, *Tectonophysics*, *343*, 79–92, 2001.

Katz, B., R. D. Elmore, M. Cogoini, and S. Ferry, Widespread chemical remagnetization: Orogenic fluids or burial diagenesis of clays?, *Geology*, *26*, 603–606, 1998.

Katz, B., R. D. Elmore, M. Cogoini, M. H. Engel, and S. Ferry, Association between burial diagenesis of smectite, chemical remagnetization, and magnetite authigenesis in the Vocontian trough, SE France, *J. Geophys. Res.*, *105*, 851–868, 2000.

Kenis, I., P. Muchez, M. Sintubin, J. L. Mansy, and F. Lacquement, The use of a combined structural, stable isotope and fluid inclusion study to constrain the kinematic history at the northern Variscan front zone (Bettrechies, northern France), *J. Struct. Geol.*, *22*, 589–602, 2000.

Kent, D. V., Thermoviscous remagnetization in some Appalachian limestones, *Geophys. Res. Lett.*, *12*, 805–808, 1985.

Kirschvink, J. L., The least squares line and plane and the analysis of paleomagnetic data, *Geophys. J. R. Astron. Soc.*, *62*, 699–718, 1980.

Lewchuk, M. T., and D. T. A. Symons, Age and duration of Mississippi valley-type ore mineralizing events, *Geology*, *23*, 233–236, 1995.

Loucks, V., and R. D. Elmore, Absolute dating of dedolomitization and the origin of magnetization in the Cambrian Morgan Creek Limestone, central Texas, *Geol. Soc. Am. Bull.*, *97*, 486–489, 1986.

Lowrie, W., Identification of ferromagnetic minerals in a rock by coercivity and unblocking temperature properties, *Geophys. Res. Lett.*, *17*, 159–162, 1990.

Lünenschloss, B., U. Bayer, and P. Muchez, Coalification anomalies induced by fluid flow at the Variscan thrust front: A numerical model of the paleotemperature field, *Geol. Mijnbouw*, *76*, 271–275, 1997.

Márton, E., J. L. Mansy, O. Averbuch, and L. Csontos, The Variscan belt of Northern France-Southern Belgium: Geodynamic implications of new palaeomagnetic data, *Tectonophysics*, *324*, 57–80, 2000.

Matte, P., Accretionary history and crustal evolution of the Variscan belt in western Europe, *Tectonophysics*, *196*, 309–337, 1991.

McCabe, C., and J. E. T. Channell, Late Paleozoic remagnetization in limestones of the Craven Basin (northern England) and rock magnetic fingerprint of remagnetized sedimentary carbonates, *J. Geophys. Res.*, *99*, 4603–4612, 1994.

McCabe, C., and R. D. Elmore, The occurrence and origin of Late Paleozoic remagnetization in the sedimentary rocks of North America, *Rev. Geophys.*, *27*, 471–494, 1989.

Molina Garza, R. S., and J. D. A. Zijderveld, Paleomagnetism of Paleozoic strata, Brabant and Ardennes Massifs, Belgium: Implications of prefolding and postfolding Late Carboniferous secondary magnetizations for European apparent polar wander, *J. Geophys. Res.*, *101*, 15,799–15,818, 1996.

Muchez, P., M. Sintubin, and R. Swennen, Origin and migration pattern of palaeofluids during orogeny: Discussion on the Variscides of Belgium and northern France, *J. Geochem. Explor.*, *69–70*, 47–51, 2000.

Mullender, T. A. T., A. J. van Velzen, and M. J. Dekkers, Continuous drift correction and separate identification of ferrimagnetic and paramagnetic contributions in thermomagnetic runs, *Geophys. J. Int.*, *114*, 663–672, 1993.

Nielsen, P., R. Swennen, P. Muchez, and E. Keppens, Origin of Dinantian zebra dolomites south of the Brabant-Wales Massif, Belgium, *Sedimentology*, *45*, 727–743, 1998.

Oliver, J., Fluids expelled tectonically from orogenic belts: Their role in hydrocarbon migration and other geologic phenomena, *Geology*, *14*, 99–102, 1986.

Oncken, O., C. von Winterfeld, and U. Dittmar, Accretion of a rifted passive margin: The Late Paleozoic Rhenohercynian fold and thrust belt Middle European Variscides, *Tectonics*, *18*, 75–91, 1999.

Palmer, A. R., and J. Geissman, Geologic time scale, chart, Geol. Soc. of Am., Boulder, Colo., 1999. (Available at www.geosociety.org/science/timescale/timescl.pdf)

Parry, L. G., Magnetization of immobilized particle dispersions with two distinct particle sizes, *Phys. Earth Planet. Inter.*, *28*, 230–241, 1982.

Peters, C., and M. J. Dekkers, Room temperature magnetic parameters as a function of concentration, grainsize and mineralogy, *Phys. Chem. Earth*, in press, 2003.

Pique, A., S. Huon, and N. Clauer, La schistosite Hercynienne et le metamorphisme associe dans la valee de la Meuse, entre Charleville-Mezieres et Namur (Ardenne Franco-Belges), *Bull. Soc. Belge Geol.*, *93*, 55–70, 1984.

Robion, P., C. Kissel, D. Frizon de Lamotte, J. P. Lorand, and J. C. Guézou, Magnetic mineralogy and metamorphic zonation in the Ardennes Massif (France-Belgium), *Tectonophysics*, *271*, 231–248, 1997.

Rochette, P., G. Fillion, and M. J. Dekkers, Magnetic transition at 30–34 Kelvin in pyrrhotite: Insight into a widespread occurrence of this mineral in rocks, *Earth Planet. Sci. Lett.*, *98*, 319–328, 1990.

Rutter, E. H., The kinetics of rock deformation by pressure solution, *Philos. Trans. R. Soc. London, Ser. A*, *283*, 203–219, 1976.

Schroyen, K., Evolution of metamorphic fluids at the Variscan fold-and-thrust belt in eastern Belgium, *Sediment. Geol.*, *131*, 163–180, 2000.

Suk, D., D. R. Peacor, and R. Van der Voo, Replacement of pyrite framboids by magnetite in limestone and implications for paleomagnetism, *Nature*, *345*, 611–613, 1990.

Symons, D. T. A., and D. F. Sangster, Late Devonian paleomagnetic age for the Polaris Mississippi Valley-type Zn-Pb deposit, Canadian Arctic Archipelago, *Can. J. Earth Sci.*, *29*, 15–25, 1992.

Symons, D. T. A., M. T. Lewchuk, and D. L. Leach, Age and duration of the Mississippi Valley-type mineralizing fluid flow event in the Viburnum Trend, southeast Missouri, U.S.A., determined from paleomagnetism, in *Dating and Duration of Fluid Flow and Fluid-Rock Interaction*, edited by J. Parnell, *Geol. Soc. Spec. Publ., 144*, 27–39, 1998.

Tauxe, L., T. A. T. Mullender, and T. Pick, Potbellies, wasp-waists, and superparamagnetism in magnetic hysteresis, *J. Geophys. Res.*, *101*, 571–583, 1996.

Taylor, L. A., The Fe-S-O system. Oxidation of pyrrhotite and the formation of anomalous pyrrhotite, *Year Book Carnegie Inst. Washington*, *70*, 287–289, 1971.

Thominski, H. P., J. Wohlenberg, and U. Bleil, The remagnetization of Devono-Carboniferous sediments from the Ardenno-Rhenish Massif, *Tectonophysics*, *225*, 411–431, 1993.

Torii, M., K. Fukuma, C. S. Horng, and T. Q. Lee, Magnetic discrimination of pyrrhotite- and greigite-bearing sediment samples, *Geophys. Res. Lett.*, *23*, 1813–1816, 1996.

Torsvik, T. H., M. A. Smethurst, J. G. Meert, R. V. van der Voo, W. S. McKerrow, M. D. Brasier, B. A. Sturt, and H. J. Walderhaug, Continental breakup and collision in the Neoproterozoic and Paleozoic—A tale of Baltica and Laurentia, *Earth Sci. Rev.*, *40*, 229–258, 1996.

Tucker, R. D., D. C. Bradley, C. A. Verstraeten, A. G. Harris, J. R. Ebert, and S. R. McCutcheon, New U-Pb zircon ages and the duration and devision of Devonian time, *Earth Planet. Sci. Lett.*, *158*, 175–186, 1998.

Van Velzen, A. J., and J. D. A. Zijderveld, Effects of weathering on single-domain magnetite in Early Pliocene marine marls, *Geophys. J. Int.*, *121*, 267–278, 1995.

Weibel, R., Effects of burial on the clay assemblages in the Triassic Skagarrak Formation, Denmark, *Clay Miner.*, *34*, 619–635, 1999.

Weil, A. B., and R. Van der Voo, Insights into the mechanism for orogen-related carbonate remagnetization from growth of authigenic Fe-oxide: A scanning electron microscopy and rock magnetic study of Devonian carbonates from northern Spain, *J. Geophys. Res.*, *107*(B4), 2063, doi:10.1029/2001JB000200, 2002.

Xu, W., R. van der Voo, and D. R. Peacor, Electron microscopic and rock magnetic study of remagnetized Leadvillle carbonates, central Colorado, *Tectonophysics*, *296*, 333–362, 1998.

Zijderveld, J. D. A., A. C. demagnetization of rocks: Analysis of results, in *Methods on Paleomagnetism*, edited by D. W. Collinson, K. M. Creer, and S. K. Runcorn, pp. 245–286, Elsevier Sci., New York, 1967.

Zwing, A., V. Bachtadse, and H. C. Soffel, Late Carboniferous remagnetisation of Palaeozoic rocks in the NE Rhenish Massif, Germany, *Phys. Chem. Earth*, *27*(25–31), 1179–1188, 2002.

S. Bailly, M. J. Dekkers, and T. E. Zegers, Utrecht University, Faculty of Earth Sciences, Geodynamic Research Institute, Paleomagnetic Laboratory Fort Hoofddijk, Utrecht University, Budapestlaan 17, NL-3584 CD Utrecht, Netherlands. (tanja@geo.uu.nl)